Chapter 3

Fabrication and Characterization of Polyvinyl Alcohol-Soy Protein Composite Hydrogels for Skin Tissue Engineering

3.1 Introduction

Hydrogels are hydrophilic water-absorbing 3D matrices of cross-linked polymer chains used as a drug/cell/bioactive molecule delivery vehicle and tissue implant and surface coating material for biomedical applications (Chien, Chung, and Shah 2013). Although various polymers including natural and synthetic ones have been utilized for hydrogel formation, protein-based natural polymers are more advantageous since they are similar to the constituents of the ECM and thus enhance cell proliferation. However, they usually lack necessary mechanical strength. On the other hand, synthetic polymers are widely used in biomedical applications; however, due to the lack of cell adhesion moieties, their application for TE applications is quite limited (Zhang et al. 2015). Therefore, in order to improve the biological properties of synthetic polymers and overcome the poor mechanical strength of natural polymers, various combinations of these two types of polymers have been developed to achieve the synergetic effects of their individual properties in a composite material (LAZZERI 1996; Cascone et al. 2001).

Due to its properties such as biodegradability, stability, mechanical strength, biocompatibility, hydrophilicity, etc., PVA has numerous biomedical applications. However, pure PVA is unsuitable for cell adhesion and protein adsorption (Gupta, Webster, and Sinha 2011; Nuttelman, Henry, and Anseth 2002). Therefore, as a scaffold biomaterial for TE applications, PVA is generally used in combination with natural polymers such as gelatin (Choi et al. 2013), chitosan (Vrana et al. 2008), starch (Bursali et al. 2011), etc. SPI is a well-known natural plant protein polymer that promotes cell adhesion and proliferation. It has emerged as a potential alternative to synthetic and animal-origin polymers and is utilized in numerous applications such as edible films, packaging, biomedical, etc. due to its magnificent properties, viz., high abundancy, excellent biocompatibility, biodegradability, and hydrophilicity. Some studies have been

reported in the literature regarding its use and potential benefits in numerous TE applications (Santin and Ambrosio 2008; Merolli et al. 2010). Moreover, it has been reported that for tissue regeneration and wound healing, certain amino acids are essential. These include glutamine, which is utilized by inflammatory cells as an energy source for growth and proliferation, and arginine, which is essential for effective immune functions as well as wound reconstruction processes (MacKay and Miller 2003; Y, Y, and A 2008). Incidentally, these amino acids are abundantly present in SPI. However, the poor mechanical properties of SPI have restricted its profound use (D. Cho, Netravali, and Joo 2012). It consists of many polar groups containing amino acids such as aspartic acid, cysteine, glutamic acid, lysine, and arginine, which can be useful for its chemical and physical modifications. In the present work, the inferior mechanical property of SPI has been overcome by adding a PVA polymer.

Freeze-thaw method provides certain advantages over the other existing methods such as radiation-induced, enzymatic, and chemical cross-linking (Hassan and Peppas 2000). It is a simple process that does not require high temperatures or any chemical treatment. In this work, we have made an effort to prepare PVA/SPI composite hydrogel-based tissue-engineered scaffolds by mixing PVA with SPI.

The formation of PVA hydrogels using a freeze-thaw method was first reported by Peppas (Peppas 1975). During the freeze-thaw process, PVA gets crystallized and develops a well-interconnected porous architecture. This is because the water in the PVA solution works as a porogen during the freeze-thaw process and produces pores after gelation. Subsequently, lyophilization (freeze-drying) is utilized to remove the water from the hydrogel to prepare porous scaffolds for various biological and TE applications. However, the polymer network inside the PVA hydrogel generally shrinks after lyophilisation, which leads to the collapse of the pores (Qian and Zhang 2011). This

unfavourably affects the diffusion of a nutrient medium, cell growth, and its survival within the hydrogel. This is because in general, cells require space and a surface having acceptable or sufficient cellular affinity, similar to the ECM for attachment and proliferation, and optimum mechanical strength for primary support. Therefore, for TE applications, stable pore-structured PVA-based hydrogels with cell attachment moieties are necessary. Hence, they are commonly used in combination with natural polymers that can facilitate preliminary cell adhesion and growth. These blends of PVA have shown excellent properties such as biocompatibility, mechanical strength, and biodegradability(Su et al. 2010; Won et al. 2015) and thus exhibit excellent potential for widespread applications in TE and related domains.

In the literature, fabrication of PVA hydrogels using the freeze-thaw method has been reported by some researcher groups (Fathi et al. 2011; Vrana et al. 2008; S. H. Cho, Oh, and Lee 2005). However, to the best of our knowledge, no work in the literature has reported the fabrication of an SPI-based hydrogel using the freezing-thawing technique. This study employs the freeze-thaw or cryogelation method because it readily produces a highly elastic interconnected 3D macroporous network. It is also one of the most simple and easy-to-use techniques to fabricate robust materials with desired properties.

In the present work, PVA/SPI composite hydrogels have been fabricated using a facile freeze-thaw method and without the use of any cross-linker. All the fabricated hydrogels were morphologically studied through SEM images, and their pore sizes were measured using ImageJ software. Effective porosity was measured using the liquid displacement method. ATR-FTIR spectroscopy analysis was carried out to examine the intermolecular interactions. The prolonged stability and swelling ability of hydrogels were evaluated in PBS solution. Furthermore, in vitro stability and degradation were also studied in a lysozyme solution at 37 ºC. The thermal analysis of samples was performed using TGA

and DSC. Cell viability and the extent of proliferation within the hydrogels were investigated experimentally through culturing fibroblast cells and performing the MTT assay. Moreover, mechanical testing of samples was performed to investigate the strength of physically cross-linked prepared scaffolds. Additionally, the water vapor transmission rate (WVTR) of hydrogels was calculated to authenticate their potentiality in the field of skin tissue engineering. Furthermore, the potency of prepared hydrogels as a wound dressing material was examined using a full-thickness wound healing rat model.

3.2 Materials and methods

3.2.1 Materials

SPI powder was purchased from A.M. NUTRATECH Pvt., Ltd., India. PVA (average molecular weight: 60,000−125,000 g/mol) was procured from HiMedia, India. PBS, trypsin (0.25%)−EDTA (0.038%), FBS, DMEM high glucose, antibiotics penicillin and streptomycin solution, MTT assay kit, 4% paraformaldehyde, trypan blue, DAPI, DMSO, and Triton X-100 were purchased from HiMedia, India. Petri dishes (35 mm) of TARSON, centrifuge tubes, and 96-well plates of GENETIX were used. Pure distilled water and high-analytical-grade absolute ethanol (99.9%) were used in this work.

3.2.2 Synthesis of hydrogels

PVA/SPI based hydrogels were fabricated through repeated freeze−thawing cycles. PVA/SPI hydrogels with 10% (w/v) total polymer concentration were synthesized with five different ratios, viz., 100/0, 90/10, 70/30, 50/50, and 0/100 (Table 3.1). Note that to evaluate the effects of these two constituent polymers on the properties of the fabricated PVA/SPI composite hydrogels such as pore size, porosity, mechanical strength, and the ability to promote cell attachment and growth, hydrogels of different compositions with SPI concentrations of ≤50% have been fabricated in this study. This is because SPI

concentrations of >50% led to gel instability, resulting in the formation of unstable hydrogels. This is well evident from the gel fraction, mechanical properties, stability, and degradation studies reported in this work that as the concentration of SPI increases, the strength of the fabricated hydrogel decreases. In brief, first, PVA was dissolved in distilled water (pH ~7) at 121 °C in an autoclave (Life Science, India) to form a PVA solution of pH ~6.7. Thereafter, SPI powder was added and the mixture was continuously stirred at 60 °C for 1 h, which resulted in an increase in pH of the solution to ~7.8. The solution was then cooled to room temperature and poured into cylindrical molds. Subsequently, it was frozen at −20 °C for 12 h followed by thawing at room temperature for 12 h. This process was repeated for six consecutive cycles. Because of freeze-thaw cycles, physical cross-linking occurred within the samples. For performing some characterizations, all the samples were freeze-dried using the lyophilization technique (Lyophilizer, Telstar Lyo Quest). A schematic of the fabrication process of PVA/SPI hydrogels and the prepared hydrogel images are presented in Figure 3.1, Figure 3.2, and Figure 3.3 (a), respectively.

Table 3.1 Formulations of freeze-thawed PVA/SPI composite hydrogels.

Sample (10% w/v)	PVA (g)	SPI (g)	Water (mL)
100% PVA	1.00	0.00	10
90/10 PVA/SPI	0.90	0.10	10
70/30 PVA/SPI	0.70	0.30	10
50/50 PVA/SPI	0.50	0.50	10
100% SPI	0.00	1.00	10

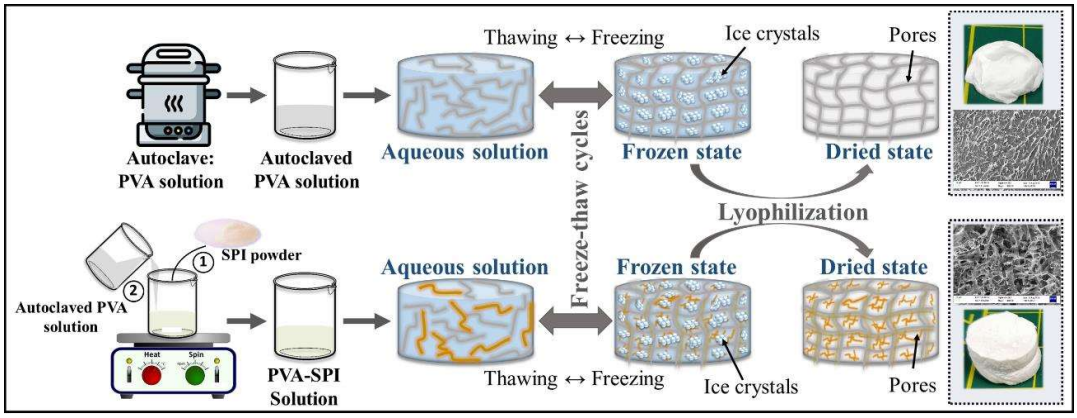

Figure 3.1 Schematic representation of fabrication process of FT PVA/SPI scaffolds.

Figure 3.2 Digital images fabricated all FT PVA/SPI hydrogels: before freeze-thawing, after freeze-thawing and after lyophilisation.

3.2.3 Characterization of the hydrogels

3.2.3.1 Gel Fraction

The gel fraction (GF) is the ratio of the weight of the dried cross-linked polymer structure to the dry weight of the polymer structure before soaking in a suitable solvent (Wong, Ashton, and Dodou 2015b). The cylindrical-shaped samples were dried using a

lyophilization technique for 12 h. Dried samples were immersed in distilled water for 24 h. The samples were then removed from the solution to separate the soluble parts. Thereafter, the samples were again freeze-dried for 12 h (Hwang et al. 2010). The GF percentage was calculated as

$$GF\ (\%) = \left(\frac{W_g}{W_i}\right) \times 100, \tag{3.1}$$

where W_i is the dry weight of the sample prior to immersion and W_g is the dry weight of the same sample after 24 h of immersion.

3.2.3.2 Porosity

The porosity of fabricated hydrogels was measured using the liquid replacement method (Varshney et al. 2019). The freeze-dried cylindrical-shaped samples were weighed (W_D) and then immersed in absolute EtOH, which is not a solvent for the hydrogels. All submerged samples were subjected to EtOH permeation using frequent cycles of evacuation-repressurization in a vacuum desiccator. The weight of the saturated hydrogels was denoted as W_W, and the porosity was calculated as

$$Porosity\ (\%) = \left(\frac{V_S}{V_H}\right) \times 100, \tag{3.2}$$

and V_S was determined using the equation given below:

$$V_S = \left(\frac{W_W - W_D}{\rho_E}\right), \tag{3.3}$$

where V_S is the sample-permeated EtOH volume and V_H is the apparent volume, which is calculated from the measured dimensions of the hydrogel samples. ρ_E is the EtOH density (0.789 g/cm^3).

3.2.3.3 Surface wettability

To analyze the hydrophilicity of the prepared lyophilized PVA/SPI hydrogels, the contact angle (CA) was measured using the image analysis method through ImageJ software. Accordingly, 10 µL of deionized water was pipetted on the upper surface of samples (thickness: ~5mm) with the help of a micropipette and subsequently the image was recorded within 10 s using a digital camera. For every sample, the CA mean value with standard deviation was calculated by taking three independent experiments into consideration.

3.2.3.4 SEM analysis

The internal morphology and pore size distribution of the samples were determined using SEM. For SEM imaging (Zeiss EVO 18 SEM Zeiss, Oberkochen, Germany), the freeze-dried samples were coated with gold at 20 kV. The obtained images were utilized to examine the pore size distribution of samples using image analysis software, i.e., ImageJ (NIH, USA).

3.2.3.5 Swelling capacity

The water uptake capacity and saturation state of the hydrogels were determined by submerging the samples in a pH 7.4 PBS solution at room temperature for 48 h. Samples were weighed before and after immersion at regular intervals of time through a precision electronic weighing balance. For this purpose, the samples were first removed from the solution, blotted by a tissue paper to soak the excess water from the surface of samples, and then weighed. The swelling (%) was calculated using the expression in Equation (2.1).

The fluid uptake capacity is an essential requirement for wound dressing to provide a moist environment for facilitating fast healing (Dhivya, Padma, and Santhini 2015). The maximum water content (MWC) after achieving equilibrium was calculated as

$$\text{MWC}\ (\%) = \left(\frac{W_{eq} - W_{dry}}{W_{eq}}\right) \times 100, \quad \textbf{(3.4)}$$

where W_{eq} is the swollen weight of samples at equilibrium.

3.2.3.6 Water vapor transmission rate (WVTR)

The WVTR test of the hydrogels was performed at 37 ˚C and 60 ± 15 % relative humidity. The test was carried out in non-corrosive, airtight, and nonpermeable vials of ~15 mm diameter. The vials were filled with distilled water and the mouth of the vial was covered by samples of ~2 mm thickness and ~15 mm diameter while maintaining a minimum of ~ 5 mm gap between the sample and water. The samples were sealed with Teflon tape; the total weight of this setup (vial + sample + water + Teflon tape) was measured. Thereafter, the whole setup was placed in a hot air oven at 37 ˚C for 24 h. As a negative and positive control, we used the same vial type without any covering over the mouth and with Teflon covering, respectively. After 24 h, the setup was removed and weighed again. The WVTR was determined by the following equation:

$$\text{WVTR} = ((W_2 - W_1)/A)\ \times 24, \quad \textbf{(3.5)}$$

where, $W_1$and W_2 are the weights of the setup before and after being placed in a hot air oven, respectively, and A is the area of the sample for transmission.

3.2.3.7 Stability and degradation

The degradation rate of hydrogels was examined by immersing the samples in lysozyme solution (10^4 U/mL) and PBS solution (pH 7.4) at 37 ˚C and room temperature,

respectively. The dry weight of freeze-dried samples was measured followed by immersion in the respective solutions. The lysozyme degradation of samples was observed over 14 days, while the solution was replaced by fresh solution after every 2 days. Samples were withdrawn from the solution at two time points, i.e., 7^{th} and 14^{th} days and washed twice with distilled water. The weight loss percentage of the hydrogel was calculated using the expression in Equation (2.2).

3.2.3.8 ATR-FTIR spectroscopy analysis

Infrared spectra (ALPHA BRUKER Eco-ATR equipped with a ZnSe attenuated total reflection (ATR) accessory) were recorded within the range of 500– 4000 cm^{-1} and 4 cm^{-1} resolution with 24 scans. FTIR was utilized to study the effect of the freeze-thaw cycles on the samples.

3.2.3.9 X-ray diffraction (XRD)

XRD patterns of all lyophilized hydrogels were measured using a Bench Top X-ray Diffraction (BT-XRD) (Rigaku Miniflex 600 Desktop X-ray Diffraction System, RIGAKU Corporation) at a 40 kV voltage and 15 mA current with Kα radiation (λ = 1.54 nm) employing a scanning rate 0.2 s per step in the 2θ range of 10º–60º.

3.2.3.10 Differential scanning calorimetry

The thermal behavior of freeze-dried fabricated hydrogels was studied by performing DSC under a N_2 atmosphere using a Mettler STAR SW 10.00 instrument. The instrument was calibrated with indium before use, and DSC curves were presented from the second heating run at a rate of 10 ˚C min^{-1} with an average 55 mL/min N_2 gas flow rate. From the obtained DSC thermograms, the glass transition temperature (T_g) and melting temperature (T_m) were measured.

3.2.3.11 Thermogravimetric analysis

TGA was performed using a TGA-50 thermogravimetric analyzer (Shimadzu (Asia Pacific) Pte, Ltd.). The experiment was carried out in the temperature range of 20 – 500 ºC with a 10 ºC/min heating rate. TGA determines the thermal stability of the material by providing the weight change with respect to time, temperature, and atmosphere.

3.2.3.12 Mechanical properties

To examine the effect of PVA and SPI content on the mechanical strength of physically cross-linked PVA/SPI hydrogels, compression tests were performed using a Shimadzu Texture Analyzer under axial compression equipped with a 500 N load cell at a loading speed of 1 mm/min. Cylindrical-shaped hydrated (with PBS solution) samples with approximately 11 mm in thickness and 11 mm in diameter were analyzed by compressive testing. Experiments were conducted with respect to American Society for Testing and Material International standards. The stiffness of each sample was determined in triplicate (n=3) at 50% compression. The compressive modulus was calculated from the average slope of the linear region of the obtained stress versus strain graph.

3.2.3.13 Cytocompatibility study

3.2.3.13.1 Microscopic analysis

The L929-RFP (red fluorescent protein) cell line was utilized for cell culture studies, which is a mouse fibroblast cell. The use of these genetically engineered cells facilitates easy visualization and evaluation of cell growth within the scaffold under a fluorescence microscope. This is because these cells emit red fluorescence upon exposure to green light (Poddar et al. 2019). The cells were cultured with a complete growth medium containing DMEM supplemented with 10% FBS and 1% penicillin/streptomycin at 37 ˚C, 5% CO_2, and 95% humidity in a CO_2 incubator (Galaxy 170S, Eppendorf, Germany). The freeze-

dried hydrogels were preincubated with a complete growth medium in a 35-mm Petri dish for an hour. After preincubation, the excess medium was removed and discarded, and the samples were left to dry in an incubator for 30 min. Subsequently, a cell density of 1×10^5 cells was seeded on the samples and the samples were then left for an hour at 37 °C in a CO_2 incubator for cell attachment. Thereafter, 2 mL of complete culture medium was added to the plates. The plates were then left for further incubation in the CO_2 incubator. During fluorescence microscopy imaging, samples were shifted regularly in a fresh Petri plate to prevent them from fluorescence interference produced by cells that have migrated and adhered to the Petri plates.

The cell attachment and morphology of cell-cultured hydrogel samples were also examined by SEM. For this purpose, NIH-3T3 cells at a density of 1×10^5 cells/sample were seeded on the prepared hydrogels. After 5 days of culture, samples were washed with PBS solution and subsequently fixed with 4% paraformaldehyde. The samples were then serially dehydrated using different ethanol concentrations ($20\% \rightarrow 40\% \rightarrow 60\% \rightarrow 80\% \rightarrow 100\%$). Dehydrated samples were air-dried and coated with gold for SEM imaging.

3.2.3.13.2 MTT assay

Cell viability on hydrogels was evaluated using NIH-3T3 cells through the MTT reduction assay. The assay was performed using the standard protocol on hydrogels with approximately 4 mm diameter placed in the wells of the 96-well plate. The lyophilized samples were first kept under ultra-violet radiation for 1 h in a biosafety cabinet for complete sterilization. Thereafter, the cells were seeded with a density of 1×10^4 cells per sample. The cells were then incubated for 2 and 4 days in a CO_2 incubator. For all the experiments, a complete nutrient medium and cells cultured without scaffold in wells were kept as negative and positive controls, respectively. At the end of incubation, the

culture medium was removed and discarded from each well. Subsequently, all the scaffolds were transferred into the fresh wells to eliminate the risk of getting false readings because of the cells that might have migrated to the bottom of the well and adhered to it at the time of incubation. Subsequently, 100 µL of MTT solution containing 90 µL of complete medium and 10 µL of MTT (5 mg/mL) was added to the individual wells, which were then incubated for 4 h. Thereafter, formazan crystals that formed inside each well were dissolved by incubating with 100 µL of DMSO in the dark for 15 min followed by gentle mixing (Poddar et al. 2019). To take optical absorbance readings, all the solution mixtures were transferred into fresh wells. The readings were taken using a multimode microplate reader (Synergy H1 hybrid, Biotek, USA) at 570 nm.

3.2.3.14 In vivo wound healing assay

The fabricated freeze-thawed scaffolds were evaluated for the in vivo wound healing assay in the full-thickness wound excision rat models. The experiment was executed after obtaining approval from the Central Animal Ethical Committee (CAEC), Banaras Hindu University, Varanasi (no. Dean/2018/CAEC/804). A total of 12 adult Wistar rats (age: 5-7 months) with weights of 150–250 g were anesthetized by intraperitoneal injection containing ketamine (35 mg/kg) and xylazine (5-10 mg/kg). Hairs were trimmed from the dorsal side, and the skin surface was cleaned with ethanol solution. Subsequently, a circular-shaped full thickness wound of approximately 12 mm in diameter was produced through skin excision. The rats were divided into four groups: group A (90/10 PVA/SPI), group B (70/30 PVA/SPI), group C (50/50 PVA/SPI) and group D (sham). Each group contained three rats ($n = 3$). However, in the above obtained results, 100% PVA showed an inadequate level of cell attachment, infiltration, growth, proliferation, pore size, and porosity due to which 100% PVA samples were not considered for the treatment. Images were taken at regular time intervals through a digital camera. The wound area was traced

on a transparent sheet and determined through a graph paper. The wound closure rate was calculated using the expression in Equation (2.3).

After 15 days, skin was excised and kept in 4% formalin for tissue fixation. Then, samples were serially dehydrated and cut into small sections followed by permeation of liquid paraffin. Thereafter, to create tissue blocks, the paraffin-permeated samples were embedded in paraffin containing molds. Blocks were sectioned (thickness ~5 µm) using a microtome and stained with H&E. Prepared slides were studied with an OLYMPUS upright bright-field microscope. Images were visualized and recorded using the ToupView 3.7 software.

3.2.3.15 Statistical analysis

The experiments were carried out in triplicate, and the results were represented as mean ± SD. For statistical analysis, ANOVA with Tukey's multiple comparison tests was performed for all the experimental data. OriginPro 2020 (OriginLab, Learning edition) was used to plot all the graphs. In fluorescence images, the background noise was subtracted using ImageJ software. To convolve the image, the Gaussian blur function was employed followed by image subtraction to remove the background noise.

3.3 Results

3.3.1 Gel fraction

PVA/SPI homogeneous solution was physically cross-linked by employing the freeze-thaw technique. In the process, no cross-linker was used since the chemical cross-linker is often detrimental to the cells or tissues. Six cycles of the freeze-thaw process were employed to obtain a stable and insoluble hydrogel. An increment in GF % was observed with increased PVA content in the hydrogels (Figure 3.3(b)). The GF of 100**%** PVA was found to be 96 ± 0.9%, which is relatively high. This indicates almost complete cross-

linking in 100% PVA hydrogels. GF values decreased to 94 ± 0.7, 86 ± 4.8, and 85.8 ± 1.7% for stable and insoluble hydrogels with 10, 30 and 50% SPI concentrations, respectively (Table 3.2). It revealed that an increase in PVA content led to notably stronger cross-linking of the polymer network in the hydrogel. This indicates that during the freeze-thaw process, the cross-linking between the SPI and PVA was weaker than that of between the PVA-PVA. In general, a lower gel fraction signifies the formation of a hydrogel with high flexibility but lower strength and weak cross-linking (Hwang et al. 2010). Thus, SPI addition causes the formation of a less cross-linked hydrogel than the 100% PVA hydrogel. Therefore, the strength and flexibility of the composite hydrogel could be controlled by varying the concentration of SPI. Moreover, weak cross-linking facilitates easy movement of the polymer chain in the hydrogel, which may be one of the reasons for significant improvement in water retention ability in composite hydrogels in comparison to 100% PVA samples as shown by swelling capacity results. However, in the case of 100% SPI samples, no cross-linking was observed in the polymeric network or we can say that water-soluble hydrogels were obtained due to which no further characterization was performed for these samples.

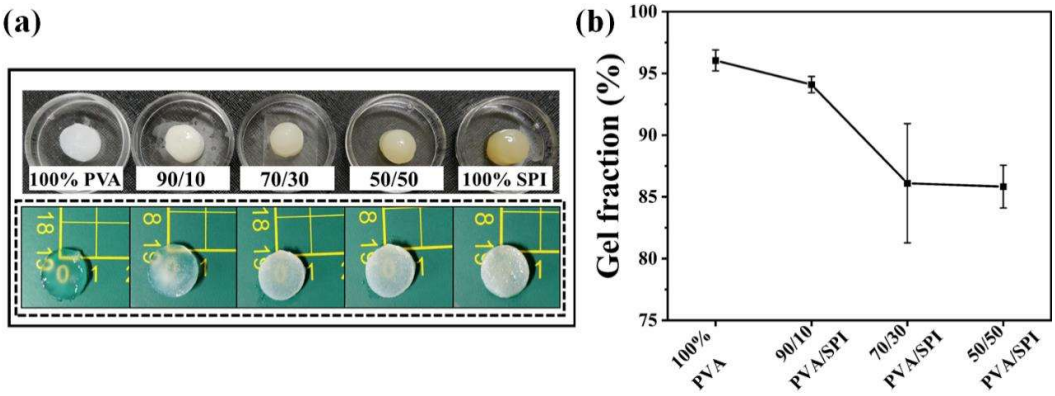

Figure 3.3 (a) Digital images of all the fabricated freeze–thawed (FT) PVA/SPI hydrogels. (b) Graph depicting gel fraction percentage. Values are expressed as mean ± SD (n = 5).

Table 3.2 Various parameters of PVA/SPI FT hydrogels with various compositions.

Parameters	100 % PVA	90/10 PVA/SPI	70/30 PVA/SPI	50/50 PVA/SPI
Gel fraction (%)	96 ± 0.9	94 ± 0.7	86 ± 4.8	85.8 ± 1.7
Average Pore Size (µm)	0.64 ± 0.43	11.7 ± 10.97	9.14 ± 13.7	15.35 ± 13.9
Porosity (%)	38 ± 4.4	56.8 ± 7.6	67 ± 5	84.1 ± 3.8
Swelling (%)	83.9 ± 9.2	118.9 ± 16.5	538.3 ± 6.3	838.8 ± 12.3
Maximum Water Content (%)	42.2 ± 5	54.1 ± 2.7	83.5 ± 1.8	89.9 ± 0.2
Average compressive Modulus (kPa)	0.201 ± 0.013	0.196 ± 0.0065	0.169 ± 0.0185	0.088 ± 0.0105

3.3.2 Porosity

Porosity plays a significant role in tissue regeneration. It quantifies the total void volume in a scaffold that is required for cell penetration and providing space for neovascularization. The porosity of the fabricated scaffolds was calculated from the total EtOH volume retained and the apparent volume of the hydrogel. A significantly higher porosity was observed in 50/50 PVA/SPI samples in comparison to other hydrogel compositions with individual values of 38 ± 4.4, 56.8 ± 7.6, 67 ± 5 and 84.1 ± 3.8% for 100% PVA, 90/10 PVA/SPI, 70/30 PVA/SPI, and 50/50 PVA/SPI hydrogels, respectively (Figure 3.4). The porosity got increased with an increase in the SPI content in hydrogels.

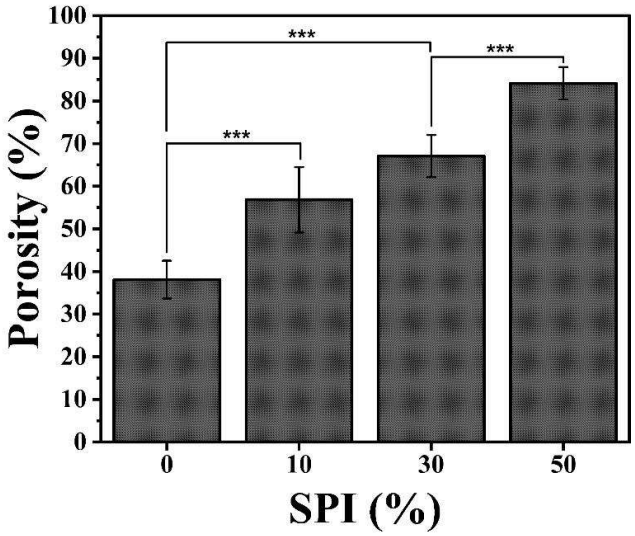

Figure 3.4 Graph depicting porosity percentage of PVA/SPI composite FT scaffolds. Values are expressed as mean ± SD (n = 5) and the level of significance as ***$p < 0.05$.

3.3.3 Surface wettability

To evaluate the surface wetting nature of samples, the water CA was measured. The CAs of 100% PVA, 90/10 PVA/SPI, 70/30 PVA/SPI and 50/50 PVA/SPI lyophilized samples were found to be 59.1 ± 8.9, 40.8 ± 4.5, 37.6 ± 2.6, and 26.5 ± 3.38˚, respectively (Figure 3.5). The respective digital images of samples in the graph show the shape of the water droplet spread on the sample surface. It is worth noting that SPI provided a supplementary water adhering property to the prepared samples. This revealed that an increase in the SPI ratio enhanced the hydrophilicity of the fabricated samples and thus resulted in a noticeable decrease in the CAs.

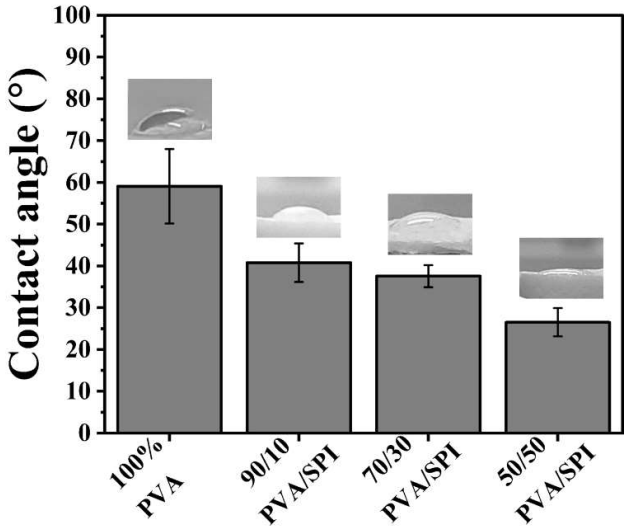

Figure 3.5 Graph depicting surface wettability of all the fabricated FT hydrogels. Values are expressed as mean ± SD (n = 5) and the level of significance as ***p < 0.05.

3.3.4 SEM analysis of the fabricated FT hydrogels

SEM analysis is a commonly used technique to study the surface topography and the characteristic network structure of hydrogels (Aikawa et al. 1998). All the fabricated SPI/PVA hydrogels were found to have a mesh-like structure of interconnected pores (Figure 3.6). The pore size of 100% PVA hydrogels was found to be smaller than the PVA/SPI composite hydrogels. The 100% PVA hydrogel showed a significant shrinkage after lyophilization, which could be observed microscopically and with the naked eye. These hydrogels showed pore sizes in the range of 0.11–2.9 μm with 0.64 ± 0.43 μm being the average pore size, while the majority of the pores had sizes in the range of 0.2–1 μm. The extent of pore size was observed to be 0.43–60 μm with an average pore size of 11.7 ± 10.97 μm in 90/10 PVA/SPI hydrogels where most of them were found to lie in the range of 10–30 μm. While the 70/30 PVA/SPI hydrogels displayed a minimum pore size of 0.42 μm and a maximum of 79 μm with an average pore size of 9.14 ± 13.7 μm, most of the pores spanned between 0.8 and 20 μm. The 50/50 PVA/SPI hydrogels exhibited pores in the range of 0.54–79 μm, whereas their maximum spanned the range

1–30 µm. The average pore size was found to 15.35 ± 13.9 µm for these hydrogels (Table 3.2).

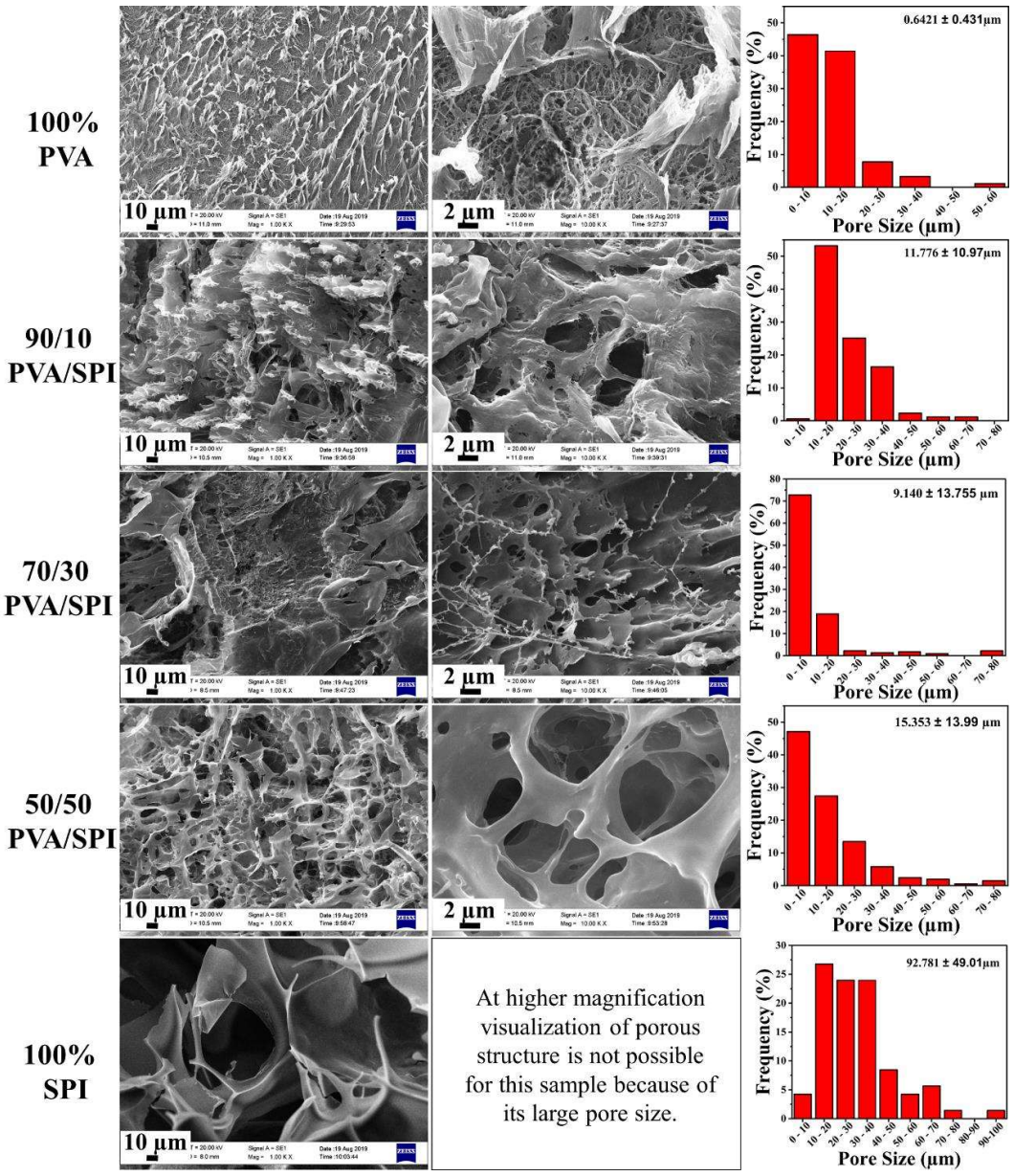

Figure 3.6 Morphological analysis through SEM photomicrographs (different magnifications) of all the prepared FT hydrogel samples with different PVA/SPI composite compositions, namely, 100% PVA, 90/10 PVA/SPI, 70/30 PVA/SPI, 50/50 PVA/SPI, and 100% SPI, along with their respective pore size distribution graphs.

The 100% SPI samples showed a comparatively larger average pore size, i.e., 92.78 ± 49.01 μm than the other prepared samples. However, no water stable structure was formed for this composition and hence these were not considered for further investigation. Thus, the pore size of hydrogels got significantly increased with an increase in the SPI content.

3.3.5 Swelling capacity

One of the basic characteristics of a hydrogel is to uptake/absorb plenty of water or medium without losing its state. This property determines the rate of diffusion of nutrients and cellular products between the hydrogel and the surrounding medium (Pan et al. 2017). Therefore, swelling is one of the most desired properties of any scaffold for TE applications. The swelling percentage of hydrogels of all the compositions increased significantly with time and attained equilibrium within 5 h of immersion (Figure 3.7 (a)). The higher content of SPI resulted in a remarkably higher swelling percentage. Moreover, due to the highly porous architecture and high hydrophilicity, the 50/50 PVA/SPI sample attained equilibrium just after 2–3 h of immersion. Furthermore, the 50/50 PVA/SPI sample showed the highest swelling percentage value i.e., 838.8 ± 12.3%, compared to other prepared hydrogel compositions (Table 3.2). The maximum water content (MWC) values obtained were 42.2 ± 5, 54.1 ± 2.7, 83.5 ± 1.8, and 89.9 ± 0.2% for 100% PVA, 90/10 PVA/SPI, 70/30 PVA/SPI, and 50/50 PVA/SPI hydrogels, respectively (Figure 3.7 (b)). The 100% SPI hydrogels were observed to start degrading and losing their integrity instantly after submerging in the PBS solution. The large amounts of water uptake make 70/30 and 50/50 PVA/SPI samples suitable as wound dressing materials for highly draining and bleeding wounds.

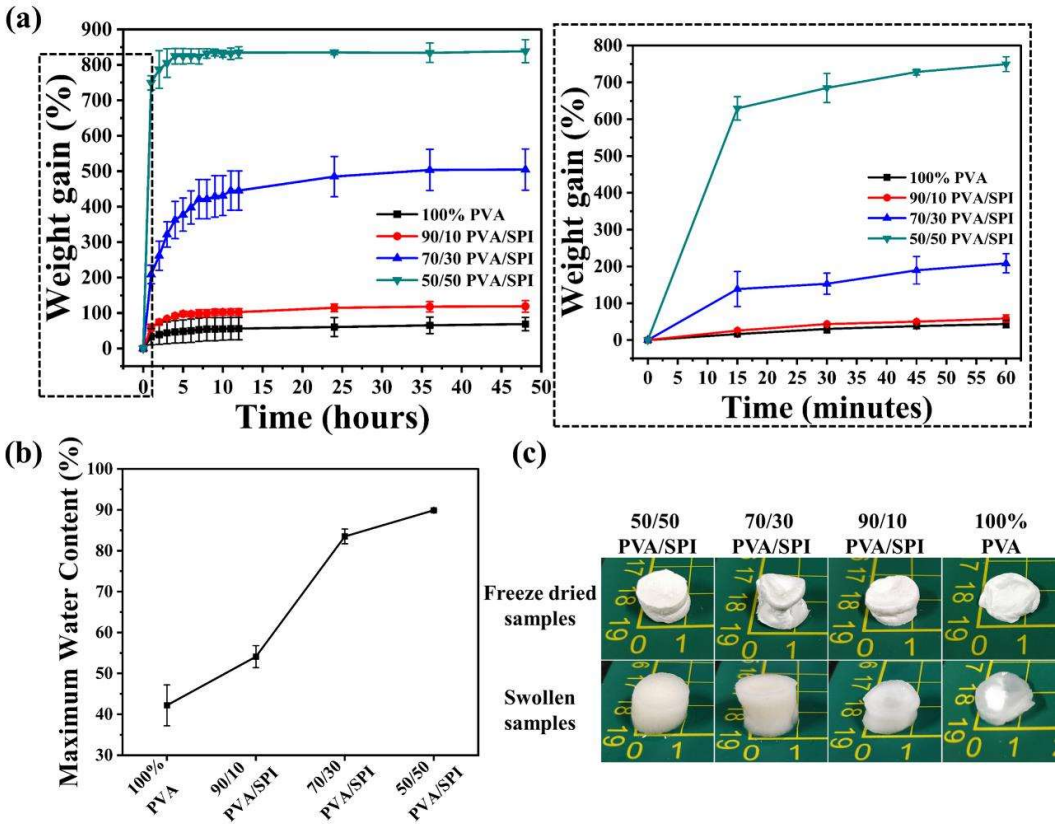

Figure 3.7 Graphs showing (a) weight gain percentage (b) maximum water content percentage of all the prepared FT hydrogel samples, namely, 100% PVA, 90/10 PVA/SPI, 70/30 PVA/SPI, and 50/50 PVA/SPI, in PBS at room temperature (25 °C). (c) Digital images of all samples after 12 h of swelling in PBS. Values are expressed as mean ± SD (n = 5). Scale bar: 10 mm.

3.3.6 Water vapor transmission rate

Permeation of water vapor is a crucial parameter for testing a scaffold's suitability for external applications such as wound dressing. An excessive loss of water through the material may cause the wound to dry, which may delay the wound healing process. For a wound dressing material, the moisture permeability should neither be too high, which may cause extreme moisture loss, nor too low, which may result in exudate leakage. Hence, the WVTR is a crucial parameter that determines the appropriateness of hydrogels specifically as a wound dressing material. The WVTRs of the different hydrogels were observed to be 2374.4 ± 95, 2405.4 ± 121, 2461.3 ± 60, 2430.8 ± 77 g $m^{-2}day^{-1}$ for 100%

PVA, 90/10 PVA/SPI, 70/30 PVA/SPI and 50/50 PVA/SPI, respectively (Figure 3.8(a)). These values show a medium permeability of the hydrogels. However, the WVTR for the control (without covering) was found to be 4997.4 ± 145 g $m^{-2}day^{-1}$, which is extremely high.

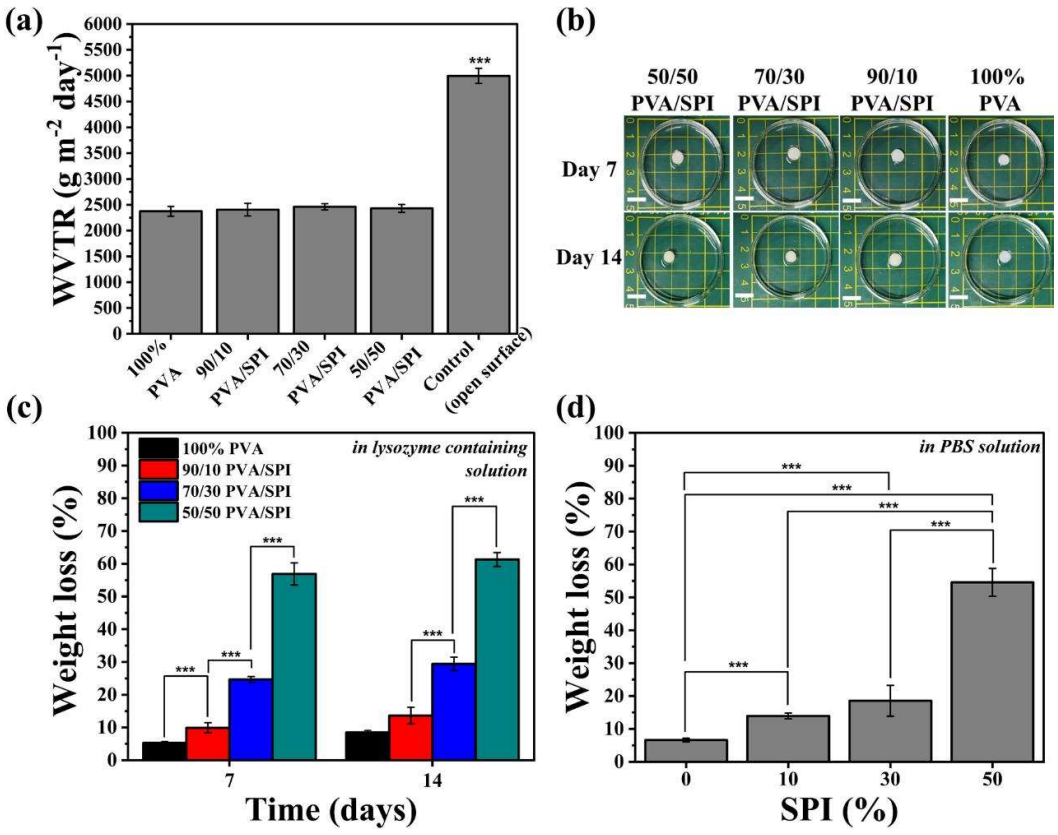

Figure 3.8 (a) Graph showing the water vapor transfer rate (WVTR). **(b)** Digital images showing FT samples (100% PVA, 90/10 PVA/SPI, 70/30 PVA/SPI, and 50/50 PVA/SPI) in PBS solution after 7 and 14 days of in vitro degradation. **(c, d)** Graphs showing weight loss percentage of all the prepared FT hydrogel samples in lysozyme-containing solution and PBS solution, respectively, at 37 °C. Values are expressed as mean ± SD (n = 3) and the level of significance as ***p < 0.05.

3.3.7 Stability and degradation of FT hydrogels

Stability and degradability are some of the most important characteristics of any scaffold that decide its applicability towards different TE areas. For many tissue regeneration

applications, the rate of degradation of the scaffold should match the rate of new tissue formation. Therefore, the material should possess controllable biodegradability to facilitate the growth of new tissue by providing the time and structure to the surrounding cells to migrate, grow, and produce their own ECM around themselves and then eventually degrade leaving behind the newly produced tissue. The cylindrical-shaped hydrogels were cut and immersed in PBS (at RT) and lysozyme solution (at 37 ºC) for 14 days. The 50/50 PVA/SPI samples were found to be about 50% degraded after 14 days of incubation in both PBS and lysozyme solutions (Figure 3.8(b-d)). Although, with digital imaging, no clear deterioration in the physical appearance of tested hydrogel samples was observed (Figure 3.8(b)), significant topographical changes, i.e., pore size and surface erosion, were confirmed in all the scaffolds after 14 days in lysozyme containing solution from SEM analysis (Figure 3.9). In PBS solution, 100% PVA, 90/10 PVA/SPI, 70/30 PVA/SPI, and 50/50 PVA/SPI showed weight loss percentages of 6.6 ± 0.6, 13.9 ± 0.9, 18.6 ± 4.7, and 54.5 ± 4.2%, respectively (Figure 3.8(d)). A similar trend was found in the lysozyme solution (Figure 3.8(c)). Moreover, it was observed that SPI addition significantly increased the degradation rate of the PVA composite hydrogel.

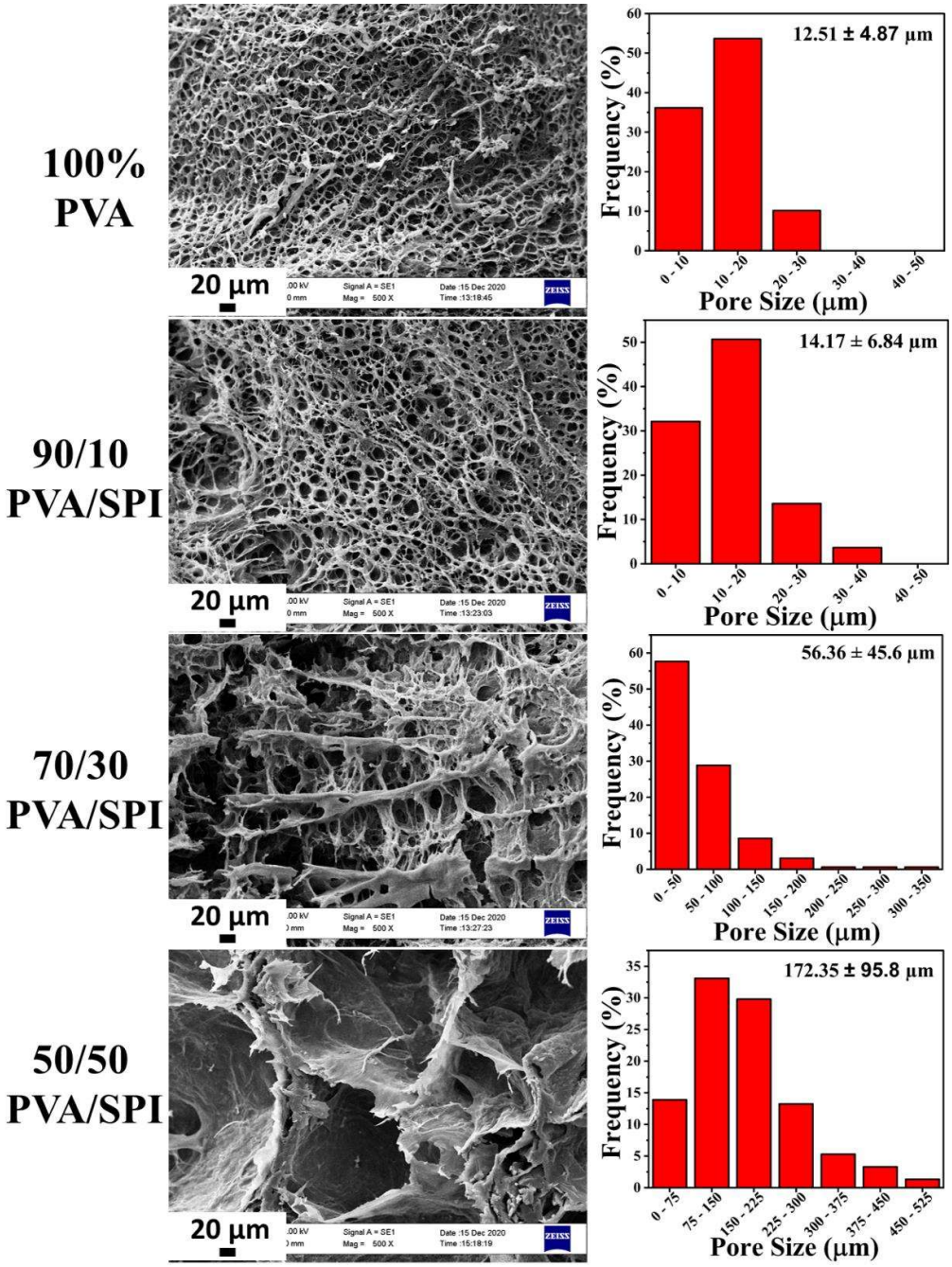

Figure 3.9 SEM micrographs along with their respective pore size distribution graphs of FT samples after 14 days of in vitro degradation in lysozyme-containing solution at 37 °C. Values are expressed as mean ± SD (n = 5) and the level of significance as ***p < 0.05.

3.3.8 ATR-FTIR spectroscopic analysis of FT Hydrogels

For an in-depth understanding of the presence of functional groups and their molecular interactions within the hydrogel, infrared analysis of the fabricated scaffolds was performed. The FTIR spectra of the 100% SPI showed major peaks at 3280, 1629, and 1520 cm^{-1} wavenumbers representing the N-H stretching vibration (amide A), C=O stretching vibration (amide I), and N-H bending (amide II), respectively (Figure 3.10(b)). In PVA, the basic structure contains -OH groups with a carbon chain. The broad absorption peak in the wavenumber range of 3275–3300 cm^{-1} was observed in all the samples, which can correspond to inter/intramolecular hydrogen bond stretching (Ceylan, Göktürk, and Bölgen 2016; Won et al. 2015). The width of the O-H stretching decreased with a corresponding decrease in the PVA concentration in hydrogels (Figure 3.10(a)). An absorption peak near the 1141 cm^{-1} wavenumber is attributed to the C-C stretching vibration as well as a characteristic of PVA crystallinity (Zhang et al. 2015; Wahid et al. 2018). The presence of the peak at 1141 cm^{-1} in PVA/SPI hydrogels indicate the crystalline domain of PVA in hydrogels. The individual peaks at 1087, 1326, 1417, and 2944 cm^{-1} correspond to the C-O stretching vibration, C-C stretching, C-H bond, and C-H stretching, respectively. As the SPI concentration increased in the hydrogels, the obtained peaks were found to be more close to 0/100 PVA/SPI peaks and vice versa for the PVA concentration.

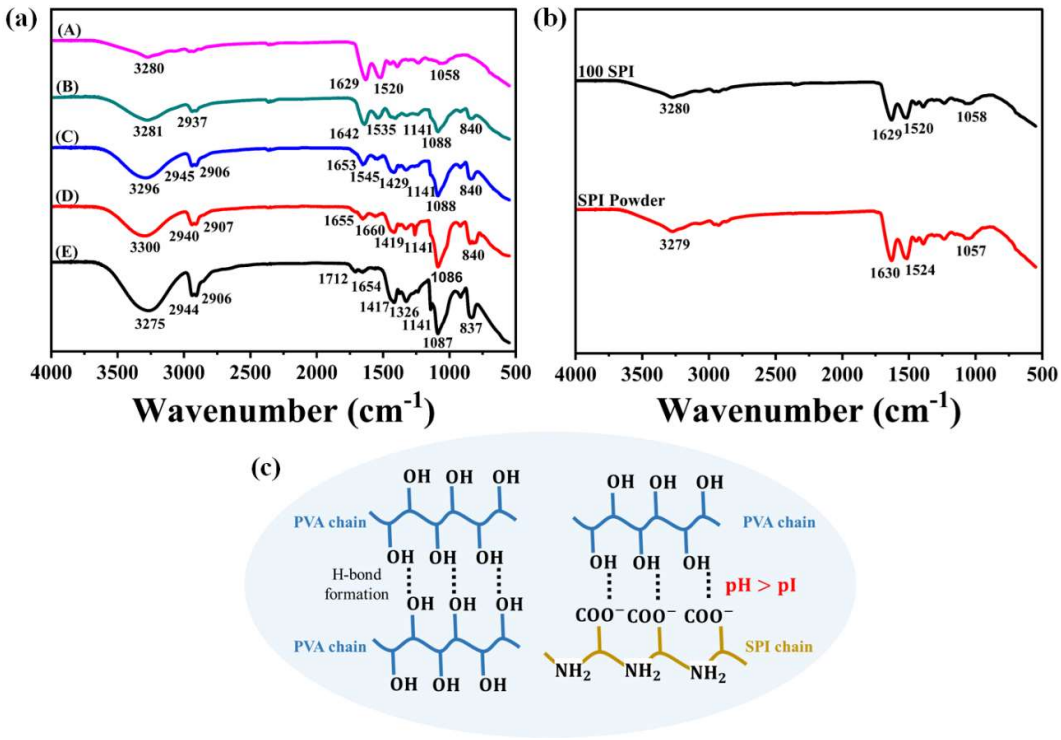

Figure 3.10 Chemical structure analysis: (a) FTIR spectra of (A) 100% SPI, (B) 50/50 PVA/SPI, (C) 70/30 PVA/SPI, (D) 90/10 PVA/SPI, (E) 100% PVA, and (b) 100% SPI FT hydrogel and SPI powder. (c) Schematic diagram representing the interaction (hydrogen bond formation) between PVA−PVA and PVA−SPI chains.

3.3.9 X-ray diffraction (XRD) analysis

The XRD patterns of 100% PVA, 90/10 PVA/SPI, 70/30 PVA/SPI, and 50/50 PVA/SPI are shown in Figure 3.11. The pattern of the PVA solid shows three characteristic peaks at 2θ = 19.1, 22.7, and 40.4°, that correspond to the crystalline planes (101), (200) and (102), respectively (Chen et al. 2018). Plane (101) generally represents the intermolecular interference between the PVA chains in the direction of intermolecular hydrogen bonding (Zhang et al. 2015; Lian and Ye 2013). A similar XRD pattern was observed in the case of each PVA/SPI hydrogel, suggesting the presence of PVA crystallites in the hydrogels. Moreover, the intensity of the peak at 19.1° decreases significantly with an increase in broadening on increasing the content of SPI. This represents reduction in crystallinity on

addition of SPI content and could be attributed to the hydrogen bond formation between the -OH groups of PVA and SPI that interfered with the PVA crystallinity. In addition, this resulted in a significant reduction of the extent of physical crosslinking of composite hydrogels, which is in coherence with the gel fraction results.

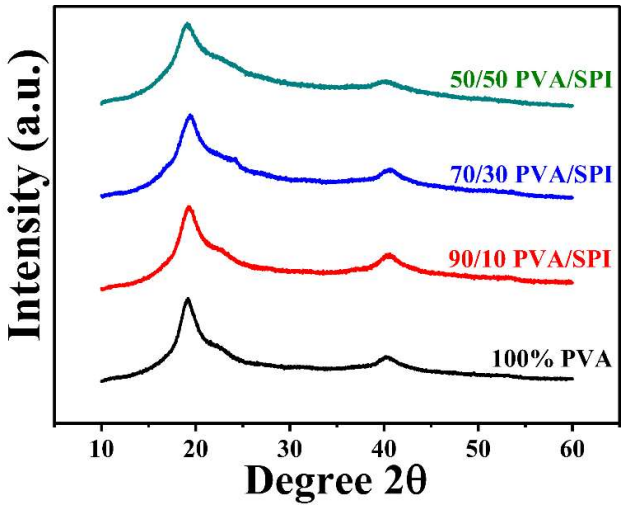

Figure 3.11 X-ray diffraction profiles of all the fabricated PVA/SPI FT hydrogels.

3.3.10 Differential scanning calorimetry analysis

The melting temperature of a polymer composite is closely related to the miscibility of its individual components. The presence of multiple melting peaks indicates the presence of two different partially miscible phases (Zhang et al. 2015). All the peaks corresponding to the melting process of the PVA/SPI samples were obtained as a single peak which signifies the good miscibility of PVA and SPI (Figure 3.12). The sharp endothermic peak at about 217 ºC determined the melting temperature (T_m) which is associated with the phase transition to liquid from solid. No significant shifting of the T_m value was observed with different compositions (Table 3.3). It was noticed that the addition of SPI to PVA caused a notable increase in glass transition temperature (T_g) from 76.0 to 87.93 ºC

(Table 3.3). The interaction of PVA and SPI chains possibly leads to an increase in the T_g value.

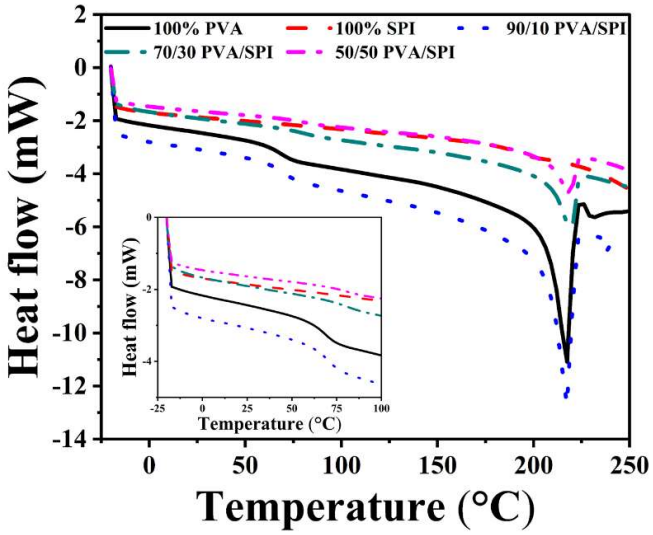

Figure 3.12 DSC curves of all the fabricated PVA/SPI FT hydrogels.

3.3.11 Thermal stability of freeze-thawed hydrogels

Thermogravimetric analysis of the lyophilized freeze-thawed hydrogels was performed to measure the mass loss of each sample with respect to temperature. The relevant TGA test results are summarized in Table 3.3. A three-step degradation process was noticed in all the samples. The initial weight loss below 100 ºC in the TGA curve occurred due to the evaporation of adsorbed and surface water from the samples. The second weight loss was observed from 225 to 411 ºC and possibly corresponded to degradation of polymer main chain. The third weight loss between 400 and 500 ºC can be attributed to pyrogenic decomposition of the remaining unstable residues. The temperature at which a sharp weight loss was recorded, called as the degradation temperature (T_d), was obtained from the endothermic peak of the derivative weight (%) curve. The T_d values of 100% PVA, 90/10 PVA/SPI, 70/30 PVA/SPI and 50/50 PVA/SPI were measured to be 305.5, 320, 332 and 325.5 ºC, respectively. Moreover, 7.02, 10.16, 25.13, 33.73% residues were

remaining at 500 ºC of 100% PVA, 90/10 PVA/SPI, 70/30 PVA/SPI and 50/50 PVA/SPI samples, respectively (Figure 3.13).

Table 3.3 Thermal properties of freeze−thawed PVA/SPI hydrogels based on DSC and TGA thermograms.

Sample	**DSC results**				**TGA results**			
	T_g (ºC)	**T_i (ºC)**	**T_f (ºC)**	**T_m (ºC)**	**T_o (ºC)**	**T_c (ºC)**	**T_d (ºC)**	**W_l (%)**
100% PVA	76.00	204.62	222.10	217.12	225.5	396.11	305.45	92.98
90/10 PVA/SPI	76.20	208.34	221.51	217.54	227.6	411.1	320.05	89.84
70/30 PVA/SPI	88.75	209.99	222.95	219.36	260.6	402.09	332.12	74.87
50/50 PVA/SPI	87.93	208.19	223.01	218.60	246.5	410.68	325.53	66.27

T_g: glass transition temperature; T_i: initial temperature of melting; T_f: end temperature of melting; T_m: melting temperature; T_o : onset thermal degradation temperature; T_c: completion thermal degradation temperature ; T_d: maximum weight loss temperature; W_l: weight loss at 500 ºC. PVA: polyvinyl alcohol; SPI: soy protein isolate.

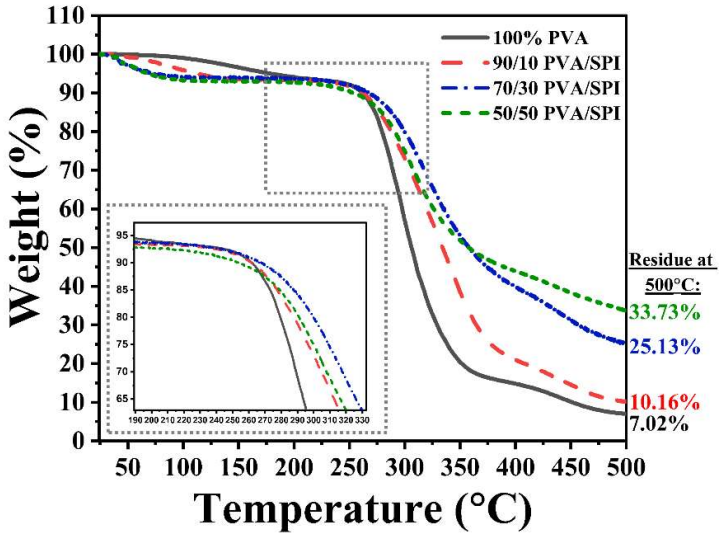

Figure 3.13 TGA graph of all the fabricated PVA/SPI FT hydrogels.

3.3.12 Mechanical properties of FT Hydrogels

For skin TE applications, the scaffold should be adequately flexible and mechanically robust enough to provide a comfortable movement and resistance from abrasion through body movement or external factors (Wong, Ashton, and Dodou 2015a). All the hydrogels were found to be elastic; they supported 50% compressive strain and regained their initial shape upon release of compressive force (Figure 3.14). However, the compressive modulus and compressive strength of the PVA/SPI composite hydrogels got decreased as the PVA content was decreased (Figure 3.14(d) and (e)). The obtained values of compressive modulus were 0.201 ± 0.013, 0.196 ± 0.0065, 0.169 ± 0.0185, and 0.088 ± 0.0105 kPa for 100% PVA, 90/10 PVA/SPI, 70/30 PVA/SPI, and 50/50 PVA/SPI, respectively (Figure 3.14(e)).

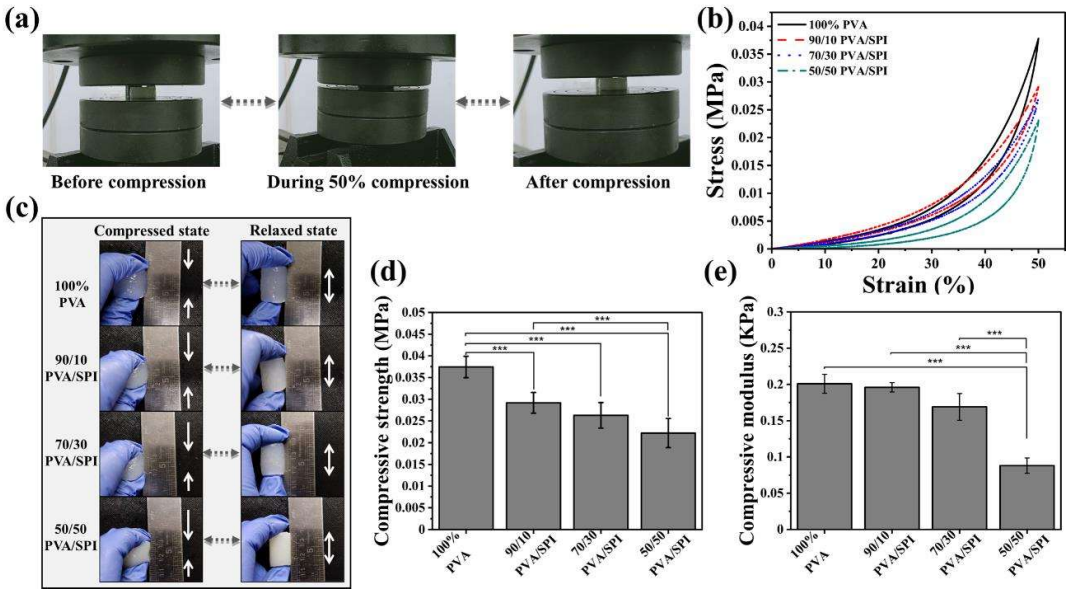

Figure 3.14 (a) Digital images of all the fabricated FT 70/30 PVA/SPI hydrogel (wet condition). (b) Compressive stress-strain curves at 50% strain under loading and unloading cycle (c) Digital images of all the fabricated FT PVA/SPI hydrogels in compressed state and in relaxed state after pressure released. Graph shows the (d) compressive strength and (e) compressive modulus values of all the fabricated PVA/SPI FT hydrogels. Values are expressed as mean ± SD (n = 3) and the level of significance as ***$p < 0.05$.

Figure 3.15 plots compressive modulus versus gel fraction (%), porosity (%), swelling (%) and pore sizes for the fabricated PVA/SPI FT hydrogels using the data given in Table 3.2. From the figure it can be observed that with an increase in gel fraction (%), the compressive modulus also increases, whereas, the compressive modulus decreases with an increase in porosity, swelling and pore size. This is in agreement with the correlation values presented in Table 3.4 below, where a positive correlation between the compressive modulus and gel fraction, and negative correlation between compressive modulus and other variables (porosity, swelling and pore sizes) can be observed.

Table 3.4: Correlation values between variables.

	Gel Fraction	**Porosity**	**Swelling**	**Pore size**
Compressive modulus	0.6967	-0.8315	-0.9338	-0.6478

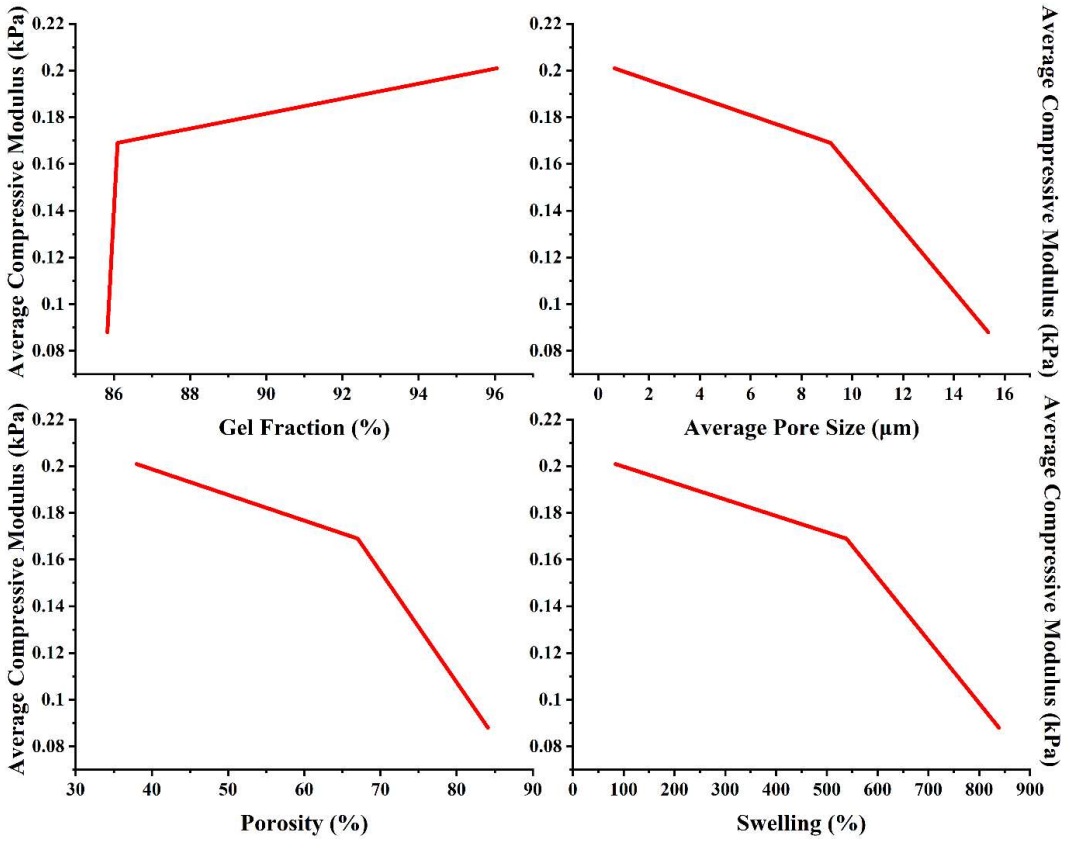

Figure 3.15: Correlation plots of compressive modulus versus gel fraction (%), porosity (%), swelling (%) and pore sizes for the PVA/SPI FT hydrogels.

To further understand the relationship between the compressive modulus and GF, porosity, swelling and pore size in the fabricated scaffold, multiple linear regression analysis using the data presented in Table 3.2 has been performed considering the regression model

$$y = \beta_0 + \beta_1 x_1 + \beta_2 x_2 + \beta_3 x_3 + \beta_4 x_4 + \epsilon \, ,$$

where y is the dependent variable (in this case compressive modulus), x_1, x_2, x_3, x_4 being the four regressor variables with $\beta_1, \beta_2, \beta_3, \beta_4$ being the corresponding regression coefficients. The quantity β_0 is the intercept and ϵ is the model error. Using the obtained regression test results (R-Square = 0.9111, F-statistic = 17.9289, P-value = 0.0009) with 95% confidence level, the null-hypothesis can be rejected and thus it can be inferred that at least one of the regressor variables contribute significantly to the model. In the future, a more comprehensive and in depth regression analysis with possibly higher order polynomial terms can be studied.

3.3.13 Cellular biocompatibility of FT hydrogels

For any TE application, cell adherence, spreading, and proliferation are the most crucial factors. To investigate the suitability of all the fabricated hydrogels for mammalian cells, L929-RFP fibroblast cells were cultured in vitro within the samples and were microscopically analyzed using fluorescence microscopy (Figures 3.16 and 3.17). It was observed from the cell culture images of lyophilized 100% PVA hydrogels that the cultured cells were sitting on the top surface of the sample with a very low cell density and poor interconnectivity between them even after 12 days of cell culture within the hydrogel. However, unlike the 100% PVA samples, enhanced cell proliferation and interconnectivity were observed within all the PVA/SPI composite hydrogels. Furthermore, fluorescence microscopy images showed that cells were growing remarkably well in 70/30 PVA/SPI and 50/50 PVA/SPI samples. SEM images of the in vitro cell culture showed that introduction of SPI in PVA hydrogels remarkably enhanced the attachment, growth and proliferation of fibroblast cells (Figure 3.18). There was no significant physical degradation of hydrogels noticed till 12 days of cell culture.

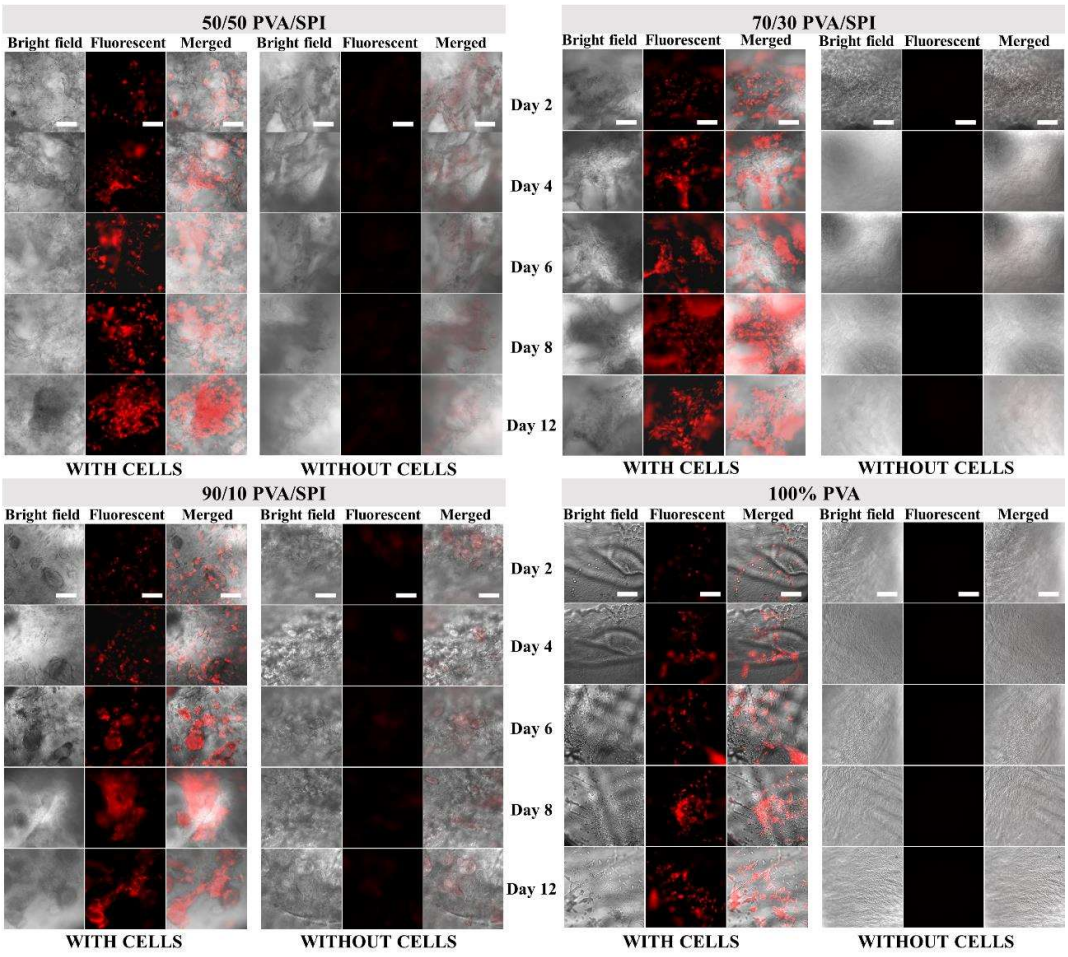

Figure 3.16 The above panel of microscopic images represents the culture of L929-RFP (fibroblast) cells within the FT scaffolds for over a period of 12 days. Scaffolds without cells were taken as control. The scale bar is 100 μm for bright-field, fluorescence, and merged images.

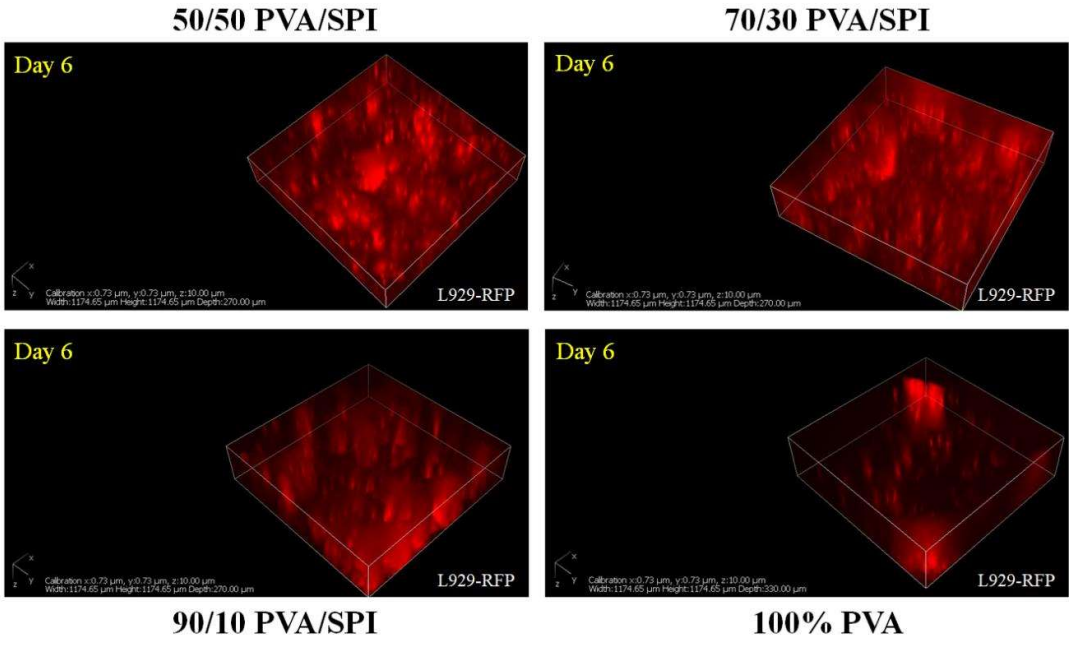

Figure 3.17 Z stacking of the images: L929-RFP cells distribution within the PVA/SPI freeze-thawed scaffolds.

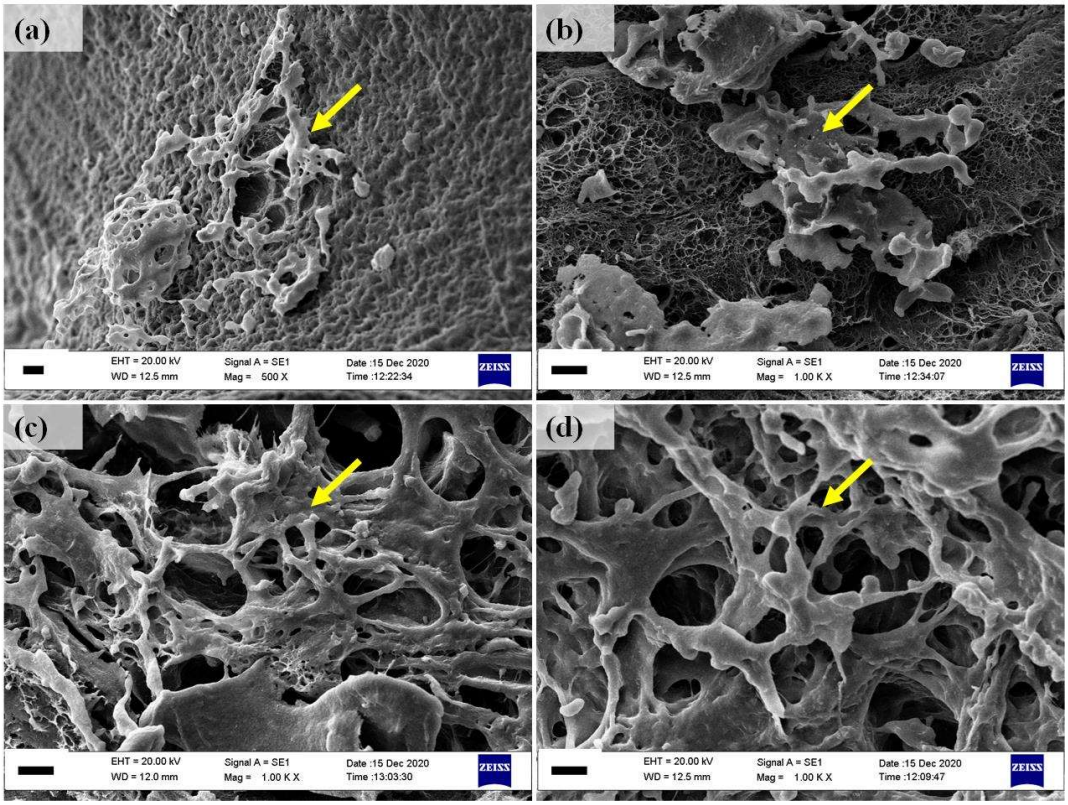

Figure 3.18 SEM images of L929-RFP (fibroblast) cells cultured on fabricated FT scaffolds: **(a)** 100% PVA, **(b)** 90/10 PVA/SPI, **(c)** 70/30 PVA/SPI, and **(d)** 50/50 PVA/SPI. Scale bar: 20 µm.

Similar results were obtained from the MTT assay (Figure 3.19). In particular, an increase in cellular viability of NIH-3T3 fibroblast cells was observed in 70/30 PVA/SPI and 50/50 PVA/SPI samples. A significant difference was found in the cell viability percentages with values of 24.4 ± 2.9, 33.8 ± 3.7, 83.4 ± 16.5 and 61.8 ± 15.4% when cultured on 100% PVA, 90/10 PVA/SPI, 70/30 PVA/SPI, and 50/50 PVA/SPI, respectively. Collectively, these observations showed that the level of cell proliferation got increased significantly upon the addition of SPI to the PVA hydrogels.

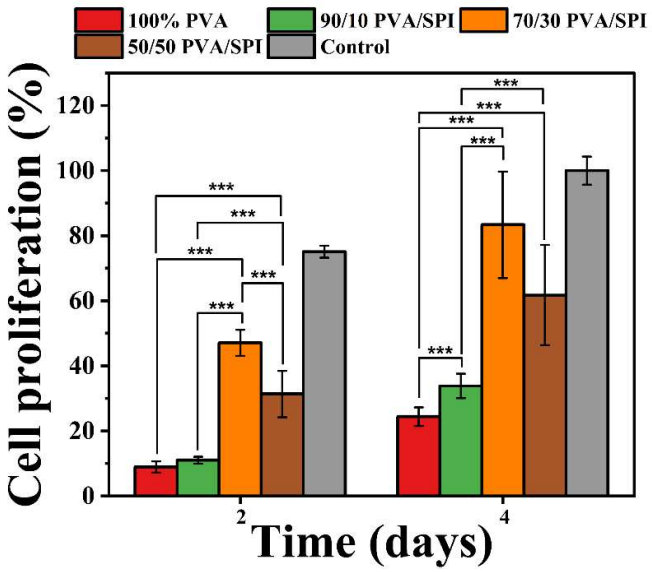

Figure 3.19 Percentage cellular viability of NIH-3T3 (fibroblast) cells and the compatibility of the scaffolds determined by the MTT assay. In the MTT assay experiment, the absorbance for the 4th day culture of positive control was taken as the reference OD for all the samples. Values are expressed as mean ± SD (n = 3) and the level of significance as ***$p < 0.05$.

3.3.14 In vivo wound healing

The preceding characterizations of the FT PVA/SPI hydrogels implied their appositeness for tissue engineering and incited us to examine their applicability as skin wound dressing. Accordingly, we investigated the healing of the full-thickness excised wound in rat models up to 15 days. It was observed that the 50/50 PVA/SPI and 70/30 PVA/SPI samples adhered excellently on the wound bed. In the case of group A (90/10 PVA/SPI), it was noticed that the sample adherence to the wound bed was notably lesser in comparison to groups B and C. All the samples degraded gradually with time. On day 9, group C (50/50 PVA/SPI) attained about 90% closure of wound, whereas group D (sham) attained closure up to 75% only. On day 13, group C (50/50 PVA/SPI) and group B (70/30 PVA/SPI) attained almost 100% closure of wound, whereas groups D and A obtained < 90% wound closure (Figure 3.20). The high SPI content and porous structure of the samples might be the reason behind the fast healing in groups B and C. Probably, during

the degradation of samples, the adhesive moieties and peptides present in soy protein got exposed to the wound site. This possibly enhanced the healing rate in comparison to the untreated samples. No adverse effects (e.g., infection, fluid confinement, bleeding of granulation tissue, sepsis, death, etc.) were observed during the experiment in any animal. After 15 days, animals were sacrificed and the histological variations in their healed tissues were then evaluated through H&E staining (Figure 3.20(b)). The 50/50 PVA/SPI and 70/30 PVA/SPI treated groups showed complete re-epithelialization and a thick epidermis layer compared to other groups. The keratinocyte cells' infiltration in epidermis and collagen deposition in the dermis layer revealed the completion of the wound healing process. The sham group showed reduced re-epithelialization compared to the treated groups.

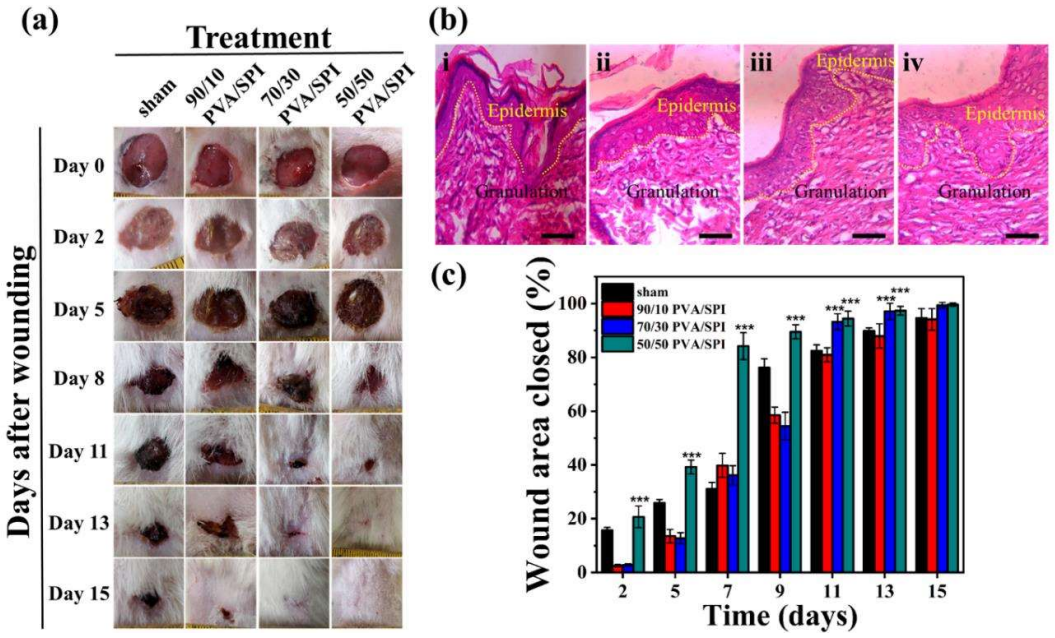

Figure 3.20 Figure showing in vivo wound healing: (a) digital photographs of full thickness wound closure on days 0, 2, 5, 8, 11, 13, and 15. (b) H&E staining image of the histological section of (i) sham, (ii) 90/10 PVA/SPI, (iii) 70/30 PVA/SPI, and (iv) 50/50 PVA/SPI after 15 days. (c) Graph depicting a comparison of wound area closed percentage of treated and sham (untreated) groups. Values are expressed as mean ± SD (n = 3) and the level of significance as ***$p < 0.05$. Scale bar: 50 μm.

3.4 Discussion

PVA is a semi-crystalline copolymer of vinyl acetate and vinyl alcohol that has been widely exploited in the chemical and medical sectors due to its biocompatibility, non-toxicity, hydrophilicity, fiber/patch-forming ability, chemical resistance, and protein adsorption (Lotfipour et al. 2019). During the freeze-thaw process, PVA gets crystallized and develops a well-interconnected porous architecture. This is because the water in the PVA solution works as a porogen during the freeze-thaw process and produces pores after gelation. SPI contains more than 90% of protein and has many reactive groups such as -NH_2, -COOH, -OH and -SH, which facilitate crosslinking with the free -OH group of PVA. SPI mainly consists of two globulin proteins: 7S (β-conglycinin) and 11S (glycinin) (Dorishetty et al. 2019). Since the solubility of these globulin proteins is reported to be very good at neutral pH and temperature range of 50–80˚C,(Sirison et al. 2017) it is therefore envisaged that SPI can show good solubility under the experimental conditions (pH > 7 at 60˚C) considered in this work. SPI has been reported to show high solubility at pH $\leq$ 3 and pH $\geq$ 6 and the least solubility at pH 4.5 = pI (isoelectric point) (Achouri, Zhang, and Shiying 1998; Hefnawy and Ramadan 2011). Possibly, during blending of PVA and SPI in distilled water at pH ~7.8, protons get extracted from the carboxylic acid of SPI to form carboxylate ions. Then, these carboxylate ions probably form strong H-bonding with the –OH group of PVA, which is also evidenced from the FTIR results. FTIR spectra of PVA/SPI show a broad and strong absorption band at ~3280–3300 cm^{-1}, which are attributed to the symmetrical stretching vibration of hydroxyl groups. This supports the formation of hydrogen bonding between PVA and SPI. The polymer chains in the prepared PVA/SPI hydrogels interact to form hydrogen bonds. This leads to the formation of a crystalline region with crystallites as physical cross-linking points in the structure. Intuitively, an increase in the SPI content is weakening the interaction between

the hydrogen bonds of PVA-PVA molecules. This is because with an increase in the SPI contents, the distance between the PVA molecules increases, resulting in a decrease in the density of –OH groups. Hence, it can be inferred from the XRD results that an increase in the SPI content leads to a decrease in physical cross-linking, which results in a decrease in the crystallinity of composite PVA hydrogels.

All the prepared hydrogels were found to be porous, soft, and elastic and had an interconnected porous structure. Results revealed that the consecutive freeze-thaw cycles produced entangled, physically cross-linked hydrogels of all the PVA/SPI homogeneous solutions (100% PVA, 90/10 PVA/SPI, 70/30 PVA/SPI, and 50/50 PVA/SPI) except for 100% SPI. The GF was found to be decreasing with a decreasing PVA concentration (Kim et al. 2008). It has been found that the porous structure of FT PVA hydrogels get deformed during the lyophilization process. This leads to a significant reduction in the porosity and pore size in the scaffolds and hence results in a significant reduction in cell growth and diffusion of nutrient medium, which are crucial for cell growth and survival. Therefore, the porous structure controllability is required in FT PVA hydrogels. During the lyophilization process, the fabricated hydrogels with a high SPI content were found to be maintaining their shape without shrinkage and deformation. A similar observation was obtained from the SEM micrographs. Therefore, it can be inferred that the addition of SPI to PVA can prevent the shrinkage of the structure and pore collapse during lyophilization. Moreover, this is in accordance with the observation made by Zhang et al. wherein they have observed that after lyophilization, the pore size gets reduced due to the shrinkage of the pore structure in a physically cross-linked PVA hydrogel, which limits its usability in TE applications. Thus, they added carrageenan (CAR) to the PVA hydrogel in order to get enhanced pore structure stability. They also showed a relationship between the CAR concentration and the pore size (Zhang et al. 2015). Similarly, in the present

work, we achieved a significant improvement in the pore size and porosity of PVA/SPI composite hydrogels with an increase in the SPI concentration.

The SEM results of freeze-dried prepared hydrogels showed interconnected microporous mesh-like structures, which play an important role in TE applications such as providing 3D spatial distribution of cells, sufficient space for storage, and transportation of nutrient medium and gases (Wong, Ashton, and Dodou 2015a). Furthermore, these structures are responsible for fast water transport, which is self-explained by results of the swelling study wherein 70/30 (PVA/SPI) and 50/50 (PVA/SPI) samples showed excellent swelling capability. These outcomes depict that the addition of SPI leads to a significant increase in the swelling of hydrogels, which is one of the key requirements for wound dressing materials to be able to absorb the excess wound exudate. This is probably because of the presence of charged amino acids (e.g., aspartic acid and glutamic acid) in high amounts compared to hydrophobic amino acids (e.g., leucine) in SPI. There are two types of wound dressings, i.e., dry and wet, and it has been reported that a moist environment remarkably enhances the healing rate in comparison to a dry environment (Jones, Grey, and Harding 2006; Winter 1962). All MWC values (42.2 ± 5 to 89.9 ± 0.2%) obtained for the prepared hydrogels were notably higher in comparison to the natural water content of normal stratum corneum, i.e., 15–30% of dry tissue weight. Thus, the fabricated PVA/SPI hydrogels could also be used as transdermal drug delivery patches due to their high water content since water can work like a natural penetration enhancer through hydration and humidity. Hydration prevents water loss from the skin that can change the water content of the stratum corneum, which facilitates the easy diffusion of drug molecules into the skin tissue (Wong, Ashton, and Dodou 2015b; Williams and Barry 2004).

The WVTR of healthy skin is nearly 204 g m^{-2} day^{-1}, whereas for the damaged skin, the value is in between 278.4 and 5138.4 g m^{-2} day^{-1} (Bajpai, Bajpai, and Gautam 2014). The wound dressing material should possess a WVTR that can protect the wound from excess exudate absorption as well as dehydration. Therefore, it has been generally recommended that an ideal wound dressing should have a WVTR ranging from 2000 to 2500 g m^{-2} day^{-1}, which is half of the granulated wound (Queen et al. 1987). The WVTR outcomes revealed that all the fabricated hydrogels had WVTR values in this ideal range. Thus, the fabricated hydrogel can be a good candidate as a wound dressing. The compressive modulus is an indicator of the extent of material flexibility and elasticity (S. H. Cho, Oh, and Lee 2005). The PVA content had a substantial effect on the mechanical properties of fabricated hydrogels since the compressive modulus of the hydrogel got significantly increased with an increase in PVA concentration. Holloway et al. have reported that in addition to the number of freeze-thaw cycles, the polymer concentration also has an important effect on mechanical properties (Holloway, Lowman, and Palmese 2012).

Both PVA and SPI are aqueous soluble, non-toxic, and biodegradable polymers. In general, the cell response to the material is influenced by its surface morphology including microstructures and their interconnectivity, surface roughness, and surface wettability (hydrophilic or hydrophobic). Cells are promoted to adhere and proliferate on hydrophilic surfaces (Wei et al. 2009; Li et al. 2016). Herein, as revealed by surface CA measurement results, the SPI incorporation significantly enhanced hydrophilicity of the composite scaffolds, thus making them appropriate for cell adhesion and proliferation. Hydrophilicity and porosity are the two sides of the same coin. Increased wettability does not always indicate that the surface is highly porous and vice versa. If the surface is hydrophilic, then there will be an increased interaction between the pore walls and the water molecules, thus influencing water permeability and a decrease in the CA. On the

other hand, if the surface is not hydrophilic in nature, then it becomes difficult for water molecules to interact with and penetrate the pores of the scaffold. Nevertheless, pore sizes in the subnanometer scale escalate the capillary force, causing a rapid infiltration of the water molecules and thus decreasing the CA significantly, which does not particularly indicate the degree of hydrophilicity or hydrophobicity of the substrate (Xu et al. 2019). Since both PVA and SPI are hydrophilic in nature, the hydrophilicity of the prepared composite hydrogels increases with an increase in SPI content and porosity. Moreover, as indicated in Table 3.2, PVA/SPI 50/50 scaffolds showed the maximum water holding capacity of approximately 90% of its original weight, which supports its applicability as a wound dressing material, drug delivery vehicle, etc.

The prepared PVA/SPI composite scaffolds provide a 3D microenvironment similar to the ECM which facilitates cell infiltration, growth, proliferation, and space for ECM deposition produced by cells to make a new tissue. In addition, it maintains the moist environment of the wounded site to accelerate the wound healing process. As both the components of the composite hydrogel are highly biocompatible, no cell toxicity was observed. From SEM images of the cell culture on the sample, 70/30 and 50/50 PVA/SPI samples showed excellent cell growth, which might be due to suitable porosity, pore sizes, pore interconnectivity, and material composition for cell infiltration, adhesion, spreading, and proliferation. Cellular biocompatibility studies evidenced that the inclusion of SPI to PVA augmented the cellular response and compatibility of composite hydrogels toward mammalian cells by aiding cell adhesion moieties. The cells on 70/30 and 50/50 PVA/SPI samples spread over the whole scaffold across the length. This shows the good cytocompatibility of composite scaffolds toward the cells because of the cell attachment- and proliferation-promoting nature of SPI. In conclusion, the hydrophilic surface promoted cell attachment, and the composition of scaffold benefited cell growth and

proliferation and the porous architecture aided nutrient transport and metabolic by-product removal. It has been speculated that degraded products of soy based scaffolds contain some cryptic peptides that play a pivotal role in enhancing the wound healing process (Har-el et al. 2014). These results are consistent with some reported studies in which the addition of SPI to different materials resulted in a significant improvement in their biocompatibility along with an enhancement in cell adhesion, growth, and proliferation. For example, Li et al. have reported that SPI and its hydrolyzed products, i.e., functional active peptides and amino acids, can enhance the in vivo or in vitro cell growth and proliferation by supplying nutrients for cell growth (Li et al. 2016). Khabbaz et al. have prepared glutaraldehyde cross-linked PVA and SPI blend electrospun nanofibrous mats and casting films for wound healing applications. From an in vitro cell culture study, they have hypothesized that these soy-based nanofibrous mats have good potential to be used in wound healing applications (Khabbaz, Solouk, and Mirzadeh 2019). Thirugnanaselvam et al. have developed a permanent wound dressing material made from SPI and PEO blend electrospun nanofibers. They observed fast wound healing in the SPI/PEO treated group due to a high amount of glutamine and arginine supply from SPI, which causes fast cell proliferation at the wound site (Thirugnanaselvam, Gobi, and Arun Karthick 2013). Thus, the prepared composite scaffolds in this study carry enormous potential as soft tissue-engineered implants.

3.5. Summary

Physically cross-linked PVA/SPI hydrogels were successfully fabricated using an easy and simple freeze-thaw technique. The porosity, swelling, degradation, and mechanical properties of the hydrogels were modulated by varying the ratio of polymers according to the application. The FT 100% SPI hydrogel was found to be unstable in water. An increase in SPI concentration led to a significant reduction in the mechanical strength,

gelation %, and stability but yielded an enhancement in the swelling capacity, degradation, pore size enlargement, cell attachment, and proliferation. The cell culture studies revealed the excellent biocompatibility of the fabricated composite scaffolds with enhanced cell attachment and proliferation. Thus, the outcomes suggest that PVA/SPI hydrogels can be an ideal candidate for TE, especially for the skin wound dressing material. The in vivo full thickness wound healing assay in rat models supported the potency of PVA/SPI hydrogels as a wound dressing material.

3.6 References

Achouri, Allaoua, Wang Zhang, and Xu Shiying. 1998. “Enzymatic Hydrolysis of Soy Protein Isolate and Effect of Succinylation on the Functional Properties of Resulting Protein Hydrolysates.” *Food Research International* 31 (9): 617–23. https://doi.org/10.1016/S0963-9969(98)00104-5.

Aikawa, K., K. Matsumoto, H. Uda, S. Tanaka, H. Shimamura, Y. Aramaki, and S. Tsuchiya. 1998. “Hydrogel Formation of the PH Response Polymer Polyvinylacetal Diethylaminoacetate (AEA).” *International Journal of Pharmaceutics* 167 (1): 97–104. https://doi.org/10.1016/S0378-5173(98)00057-X.

Bajpai, Manjula, S. K. Bajpai, and Dinesh Gautam. 2014. “Investigation of Regenerated Cellulose/Poly(Acrylic Acid) Composite Films for Potential Wound Healing Applications: A Preliminary Study.” Research Article. Journal of Applied Chemistry. Hindawi. May 6, 2014. https://doi.org/10.1155/2014/325627.

Bursali, Elif Ant, Senem Coskun, Murat Kizil, and Mürüvvet Yurdakoc. 2011. “Synthesis, Characterization and in Vitro Antimicrobial Activities of Boron/Starch/Polyvinyl Alcohol Hydrogels.” *Carbohydrate Polymers* 83 (3): 1377–83. https://doi.org/10.1016/j.carbpol.2010.09.056.

Cascone, M. G., N. Barbani, C. Cristallini P.Giusti, G. Ciardelli, and L. Lazzeri. 2001. “Bioartificial Polymeric Materials Based on Polysaccharides.” *Journal of Biomaterials Science, Polymer Edition* 12 (3): 267–81. https://doi.org/10.1163/156856201750180807.

Ceylan, Seda, Dilek Göktürk, and Nimet Bölgen. 2016. “Effect of Crosslinking Methods on the Structure and Biocompatibility of Polyvinyl Alcohol/Gelatin Cryogels.” *Bio-Medical Materials and Engineering* 27 (4): 327–40. https://doi.org/10.3233/BME-161589.

Chen, Ya-Nan, Chen Jiao, Yaxin Zhao, Jianan Zhang, and Huiliang Wang. 2018. “Self-Assembled Polyvinyl Alcohol-Tannic Acid Hydrogels with Diverse Microstructures and Good Mechanical Properties.” *ACS Omega* 3 (9): 11788–95. https://doi.org/10.1021/acsomega.8b02041.

Chien, Karen B., Eun J. Chung, and Ramille N. Shah. 2013. “Investigation of Soy Protein Hydrogels for Biomedical Applications: Materials Characterization, Drug Release, and

Biocompatibility:" *Journal of Biomaterials Applications*, July. https://doi.org/10.1177/0885328213497413.

Cho, Daehwan, Anil N. Netravali, and Yong Lak Joo. 2012. "Mechanical Properties and Biodegradability of Electrospun Soy Protein Isolate/PVA Hybrid Nanofibers." *Polymer Degradation and Stability* 97 (5): 747–54. https://doi.org/10.1016/j.polymdegradstab.2012.02.007.

Cho, Sang Ho, Se Heang Oh, and Jin Ho Lee. 2005. "Fabrication and Characterization of Porous Alginate/Polyvinyl Alcohol Hybrid Scaffolds for 3D Cell Culture." *Journal of Biomaterials Science. Polymer Edition* 16 (8): 933–47. https://doi.org/10.1163/1568562054414658.

Choi, Soon Mo, Deepti Singh, Ashok Kumar, Tae Hwan Oh, Yong Woo Cho, and Sung Soo Han. 2013. "Porous Three-Dimensional PVA/Gelatin Sponge for Skin Tissue Engineering." *International Journal of Polymeric Materials and Polymeric Biomaterials* 62 (7): 384–89. https://doi.org/10.1080/00914037.2012.710862.

Dhivya, Selvaraj, Viswanadha Vijaya Padma, and Elango Santhini. 2015. "Wound Dressings – a Review." *BioMedicine* 5 (4): 22. https://doi.org/10.7603/s40681-015-0022-9.

Dorishetty, Pramod, Rajkamal Balu, Anjitha Sreekumar, Liliana de Campo, Jitendra P. Mata, Namita Roy Choudhury, and Naba K. Dutta. 2019. "Robust and Tunable Hybrid Hydrogels from Photo-Cross-Linked Soy Protein Isolate and Regenerated Silk Fibroin." *ACS Sustainable Chemistry & Engineering* 7 (10): 9257–71. https://doi.org/10.1021/acssuschemeng.9b00147.

Fathi, Ezatollah, Nahid Atyabi, Mohamad Imani, and Zeinab Alinejad. 2011. "Physically Crosslinked Polyvinyl Alcohol–Dextran Blend Xerogels: Morphology and Thermal Behavior." *Carbohydrate Polymers* 84 (1): 145–52. https://doi.org/10.1016/j.carbpol.2010.11.018.

Gupta, Siddhi, Thomas J. Webster, and Arvind Sinha. 2011. "Evolution of PVA Gels Prepared without Crosslinking Agents as a Cell Adhesive Surface." *Journal of Materials Science: Materials in Medicine* 22 (7): 1763–72. https://doi.org/10.1007/s10856-011-4343-2.

Har-el, Yah-el, Jonathan A. Gerstenhaber, Ross Brodsky, Richard B. Huneke, and Peter I. Lelkes. 2014. “Electrospun Soy Protein Scaffolds as Wound Dressings: Enhanced Reepithelialization in a Porcine Model of Wound Healing.” *Wound Medicine* 5 (June): 9–15. https://doi.org/10.1016/j.wndm.2014.04.007.

Hassan, Christie M., and Nikolaos A. Peppas. 2000. “Structure and Applications of Poly(Vinyl Alcohol) Hydrogels Produced by Conventional Crosslinking or by Freezing/Thawing Methods.” In *Biopolymers · PVA Hydrogels, Anionic Polymerisation Nanocomposites*, 37–65. Advances in Polymer Science. Berlin, Heidelberg: Springer. https://doi.org/10.1007/3-540-46414-X_2.

Hefnawy, Hefnawy Taha Mansour, and Mohamed Fawzy Ramadan. 2011. “Physicochemical Characteristics of Soy Protein Isolate and Fenugreek Gum Dispersed Systems.” *Journal of Food Science and Technology* 48 (3): 371–77. https://doi.org/10.1007/s13197-010-0203-1.

Holloway, Julianne L., Anthony M. Lowman, and Giuseppe R. Palmese. 2012. “The Role of Crystallization and Phase Separation in the Formation of Physically Cross-Linked PVA Hydrogels.” *Soft Matter* 9 (3): 826–33. https://doi.org/10.1039/C2SM26763B.

Hwang, Ma-Ro, Jong Oh Kim, Jeong Hoon Lee, Yong Il Kim, Jeong Hoon Kim, Sun Woo Chang, Sung Gju Jin, et al. 2010. “Gentamicin-Loaded Wound Dressing With Polyvinyl Alcohol/Dextran Hydrogel: Gel Characterization and In Vivo Healing Evaluation.” *AAPS PharmSciTech* 11 (3): 1092–1103. https://doi.org/10.1208/s12249-010-9474-0.

Jones, Vanessa, Joseph E Grey, and Keith G Harding. 2006. “Wound Dressings.” *BMJ : British Medical Journal* 332 (7544): 777–80.

Khabbaz, Bahareh, Atefeh Solouk, and Hamid Mirzadeh. 2019. “Polyvinyl Alcohol/Soy Protein Isolate Nanofibrous Patch for Wound-Healing Applications.” *Progress in Biomaterials* 8 (3): 185–96. https://doi.org/10.1007/s40204-019-00120-4.

Kim, Jong Oh, Jung Kil Park, Jeong Hoon Kim, Sung Giu Jin, Chul Soon Yong, Dong Xun Li, Jun Young Choi, et al. 2008. “Development of Polyvinyl Alcohol–Sodium Alginate Gel-Matrix-Based Wound Dressing System Containing Nitrofurazone.” *International Journal of Pharmaceutics* 359 (1): 79–86. https://doi.org/10.1016/j.ijpharm.2008.03.021.

LAZZERI, L. 1996. “Progress in Bioartificial Polymeric Materials.” *Progress in Bioartificial Polymeric Materials* 4 (8): 249–52.

Li, Mingming, Yao Xiao, Yan Chen, Hong Ni, Jie Cai, Xiaomei Wang, Peter R. Chang, Debbie P. Anderson, and Yun Chen. 2016. “Soy Protein-Modified Waterborne Polyurethane Biocomposites with Improved Functionality.” *RSC Advances* 6 (16): 12837–49. https://doi.org/10.1039/C5RA25758A.

Lian, Zhe, and Lin Ye. 2013. “Effect of PEO on the Network Structure of PVA Hydrogels Prepared by Freezing/Thawing Method.” *Journal of Applied Polymer Science* 128 (5): 3325–29. https://doi.org/10.1002/app.38544.

Lotfipour, Farzaneh, Mitra Alami-Milani, Sara Salatin, Aylin Hadavi, and Mitra Jelvehgari. 2019. “Freeze-Thaw-Induced Cross-Linked PVA/Chitosan for Oxytetracycline-Loaded Wound Dressing: The Experimental Design and Optimization.” *Research in Pharmaceutical Sciences* 14 (2): 175. https://doi.org/10.4103/1735-5362.253365.

MacKay, Douglas, and Alan L. Miller. 2003. “Nutritional Support for Wound Healing.” *Alternative Medicine Review: A Journal of Clinical Therapeutic* 8 (4): 359–77.

Mbundi, Lubinda, Miguel González-Pérez, Fernando González-Pérez, Diana Juanes-Gusano, and José Carlos Rodríguez-Cabello. 2021. “Trends in the Development of Tailored Elastin-Like Recombinamer–Based Porous Biomaterials for Soft and Hard Tissue Applications.” *Frontiers in Materials* 7. https://www.frontiersin.org/article/10.3389/fmats.2020.601795.

Merolli, Antonio, Luigi Nicolais, Luigi Ambrosio, and Matteo Santin. 2010. “A Degradable Soybean-Based Biomaterial Used Effectively as a Bone Filler in Vivo in a Rabbit.” *Biomedical Materials (Bristol, England)* 5 (1): 15008. https://doi.org/10.1088/1748-6041/5/1/015008.

Nuttelman, Charles R, Scott M Henry, and Kristi S Anseth. 2002. “Synthesis and Characterization of Photocrosslinkable, Degradable Poly(Vinyl Alcohol)-Based Tissue Engineering Scaffolds.” *Biomaterials* 23 (17): 3617–26. https://doi.org/10.1016/S0142-9612(02)00093-5.

Pan, Hong, Daidi Fan, Wei Cao, Chenhui Zhu, Zhiguang Duan, Rongzhan Fu, Xian Li, and Xiaoxuan Ma. 2017. “Preparation and Characterization of Breathable Hemostatic

Hydrogel Dressings and Determination of Their Effects on Full-Thickness Defects." *Polymers* 9 (12). https://doi.org/10.3390/polym9120727.

Peppas, Nikolaos Ath. 1975. "Turbidimetric Studies of Aqueous Poly(Vinyl Alcohol) Solutions." *Die Makromolekulare Chemie* 176 (11): 3433–40. https://doi.org/10.1002/macp.1975.021761125.

Poddar, Suruchi, Piyush Sunil Agarwal, Ajay Kumar Sahi, Kiran Yellappa Vajanthri, Pallawi, K. N. Singh, and Sanjeev Kumar Mahto. 2019. "Fabrication and Cytocompatibility Evaluation of Psyllium Husk (Isabgol)/Gelatin Composite Scaffolds." *Applied Biochemistry and Biotechnology* 188 (3): 750–68. https://doi.org/10.1007/s12010-019-02958-7.

Qian, Lei, and Haifei Zhang. 2011. "Controlled Freezing and Freeze Drying: A Versatile Route for Porous and Micro-/Nano-Structured Materials." *Journal of Chemical Technology & Biotechnology* 86 (2): 172–84. https://doi.org/10.1002/jctb.2495.

Queen, D., J. D. Gaylor, J. H. Evans, J. M. Courtney, and W. H. Reid. 1987. "The Preclinical Evaluation of the Water Vapour Transmission Rate through Burn Wound Dressings." *Biomaterials* 8 (5): 367–71. https://doi.org/10.1016/0142-9612(87)90007-x.

Santin, Matteo, and Luigi Ambrosio. 2008. "Soybean-Based Biomaterials: Preparation, Properties and Tissue Regeneration Potential." *Expert Review of Medical Devices* 5 (3): 349–58. https://doi.org/10.1586/17434440.5.3.349.

Sirison, Jiraporn, Kentaro Matsumiya, Masahiko Samoto, Hiroshi Hidaka, Mitsutaka Kouno, and Yasuki Matsumura. 2017. "Solubility of Soy Lipophilic Proteins: Comparison with Other Soy Protein Fractions." *Bioscience, Biotechnology, and Biochemistry* 81 (4): 790–802. https://doi.org/10.1080/09168451.2017.1282808.

Su, Jun-Feng, Zhen Huang, Ying-Hui Zhao, Xiao-Yan Yuan, Xin-Yu Wang, and Min Li. 2010. "Moisture Sorption and Water Vapor Permeability of Soy Protein Isolate/Poly(Vinyl Alcohol)/Glycerol Blend Films." *Industrial Crops and Products* 31 (2): 266–76. https://doi.org/10.1016/j.indcrop.2009.11.010.

Thirugnanaselvam, M., N. Gobi, and S. Arun Karthick. 2013. "SPI/PEO Blended Electrospun Martrix for Wound Healing." *Fibers and Polymers* 14 (6): 965–69. https://doi.org/10.1007/s12221-013-0965-y.

Varshney, Neelima, Ajay Kumar Sahi, Kiran Yellappa Vajanthri, Suruchi Poddar, Chelladurai Karthikeyan Balavigneswaran, Arumugam Prabhakar, Vivek Rao, and Sanjeev Kumar Mahto. 2019. "Culturing Melanocytes and Fibroblasts within Three-Dimensional Macroporous PDMS Scaffolds: Towards Skin Dressing Material." *Cytotechnology* 71 (1): 287–303. https://doi.org/10.1007/s10616-018-0285-6.

Vrana, Nihal Engin, Yurong Liu, Garret Brian McGuinness, and Paul Aidan Cahill. 2008. "Characterization of Poly(Vinyl Alcohol)/Chitosan Hydrogels as Vascular Tissue Engineering Scaffolds." *Macromolecular Symposia* 269 (1): 106–10. https://doi.org/10.1002/masy.200850913.

Wahid, Mohamad Nizam Abdul, Saiful Izwan Abd Razak, Mohammed Rafiq Abdul Kadir, Rozita Hassan, Nadirul Hasraf Mat Nayan, and Khairul Anuar Mat Amin. 2018. "Influence of Citric Acid on the Physical and Biomineralization Ability of Freeze/Thaw Poly(Vinyl Alcohol) Hydrogel." *Journal of Biomaterials Applications* 33 (1): 94–102. https://doi.org/10.1177/0885328218771195.

Wei, Jianhua, Toshio Igarashi, Naoto Okumori, Takayasu Igarashi, Takashi Maetani, Baolin Liu, and Masao Yoshinari. 2009. "Influence of Surface Wettability on Competitive Protein Adsorption and Initial Attachment of Osteoblasts." *Biomedical Materials (Bristol, England)* 4 (4): 045002. https://doi.org/10.1088/1748-6041/4/4/045002.

Williams, Adrian C, and Brian W Barry. 2004. "Penetration Enhancers." *Advanced Drug Delivery Reviews*, Breaking the Skin Barrier, 56 (5): 603–18. https://doi.org/10.1016/j.addr.2003.10.025.

Winter, George D. 1962. "Formation of the Scab and the Rate of Epithelization of Superficial Wounds in the Skin of the Young Domestic Pig." *Nature* 193 (4812): 293–94. https://doi.org/10.1038/193293a0.

Won, Jong Sung, Ji Eun Lee, Da Young Jin, and Seung Goo Lee. 2015. "Mechanical Properties and Biodegradability of the Kenaf/Soy Protein Isolate-PVA Biocomposites." Research Article. International Journal of Polymer Science. Hindawi. October 19, 2015. https://doi.org/10.1155/2015/860617.

Wong, Rachel Shet Hui, Mark Ashton, and Kalliopi Dodou. 2015a. “Effect of Crosslinking Agent Concentration on the Properties of Unmedicated Hydrogels.” *Pharmaceutics* 7 (3): 305–19. https://doi.org/10.3390/pharmaceutics7030305.

Wong, Rachel Shet Hui, Mark Ashton, and Kalliopi Dodou. 2015b. “Effect of Crosslinking Agent Concentration on the Properties of Unmedicated Hydrogels.” *Pharmaceutics* 7 (3): 305–19. https://doi.org/10.3390/pharmaceutics7030305.

Xu, Fang, Mingjie Wei, Xin Zhang, Yang Song, Wei Zhou, and Yong Wang. 2019. “How Pore Hydrophilicity Influences Water Permeability?” *Research* 2019 (February). https://doi.org/10.34133/2019/2581241.

Y, Yoshie-Stark, Wada Y, and Wasche A. 2008. “Chemical Composition, Functional Properties, and Bioactivities of Rapeseed Protein Isolates.” *Food Chemistry* 107 (1): 32–39. https://doi.org/10.1016/j.foodchem.2007.07.061.

Zhang, Yabin, Lei Ye, Man Cui, Boguang Yang, Junjie Li, Hong Sun, and Fanglian Yao. 2015. “Physically Crosslinked Poly(Vinyl Alcohol)–Carrageenan Composite Hydrogels: Pore Structure Stability and Cell Adhesive Ability.” *RSC Advances* 5 (95): 78180–91. https://doi.org/10.1039/C5RA11331H.